Generation of functional posterior spinal motor neurons from hPSCs-derived human spinal cord neural progenitor cells

He Jax Xu[1,2†], Yao Yao[1,2†], Fenyong Yao[3†], Jiehui Chen[1,2†], Meishi Li[2,4†], Xianfa Yang[1,2,5], Sheng Li[1,6], Fangru Lu[4], Ping Hu[1,2,5,6,7], Shuijin He[3*], Guangdun Peng[2,4,7,8*] and Naihe Jing[1,2,5,7*] [ID]

Abstract

Spinal motor neurons deficiency results in a series of devastating disorders such as amyotrophic lateral sclerosis (ALS), spinal muscular atrophy (SMA) and spinal cord injury (SCI). These disorders are currently incurable, while human pluripotent stem cells (hPSCs)-derived spinal motor neurons are promising but suffered from inappropriate regional identity and functional immaturity for the study and treatment of posterior spinal cord related injuries. In this study, we have established human spinal cord neural progenitor cells (hSCNPCs) via hPSCs differentiated neuromesodermal progenitors (NMPs) and demonstrated the hSCNPCs can be continuously expanded up to 40 passages. hSCNPCs can be rapidly differentiated into posterior spinal motor neurons with high efficiency. The functional maturity has been examined in detail. Moreover, a co-culture scheme which is compatible for both neural and muscular differentiation is developed to mimic the neuromuscular junction (NMJ) formation in vitro. Together, these studies highlight the potential avenues for generating clinically relevant spinal motor neurons and modeling neuromuscular diseases through our defined hSCNPCs.

Keywords Motor neuron, Motor neuron differentiation, Neuromesodermal progenitors, Neuromuscular junction

[†]He Jax Xu, Yao Yao, Fenyong Yao, Jiehui Chen and Meishi Li contributed equally to this work.

*Correspondence:
Shuijin He
heshj@shanghaitech.edu.cn
Guangdun Peng
peng_guangdun@gibh.ac.cn
Naihe Jing
njing@sibcb.ac.cn
[1] State Key Laboratory of Cell Biology, CAS Center for Excellence in Molecular Cell Science, Shanghai Institute of Biochemistry and Cell Biology, Chinese Academy of Sciences, Shanghai 200031, China
[2] University of Chinese Academy of Sciences, Beijing, China
[3] School of Life Science and Technology, ShanghaiTech University, Shanghai 201210, China
[4] Center for Cell Lineage and Development, CAS Key Laboratory of Regenerative Biology, Guangdong Provincial Key Laboratory of Stem Cell and Regenerative Medicine, GIBH-HKU Guangdong-Hong Kong Stem Cell and Regenerative Medicine Research Centre, Guangzhou Institutes of Biomedicine and Health, Chinese Academy of Sciences, Guangzhou 510530, China
[5] Guangzhou Laboratory/Bioland Laboratory, Guangzhou 510005, China
[6] Xinhua Hospital affiliated to Shanghai Jiao Tong University School of Medicine, Shanghai 20023, China
[7] Institute for Stem Cell and Regeneration, Chinese Academy of Sciences, Beijing 100101, China
[8] Center for Cell Lineage and Atlas, Bioland Laboratory, Guangzhou 510005, China

Xu *et al. Cell Regeneration*   (2023) 12:15

Page 2 of 21

Background

Spinal motor neurons (MNs) which directly control muscle contractions are located in the ventral horn of spinal cord and are distributed across the anterior-posterior (AP) axis of the spinal domains from cervical, thoracic, lumbar to sacral (Sockanathan and Jessell 1998; Kanning et al. 2010). MNs loss results in a spectrum of devastating disorders such as amyotrophic lateral sclerosis (ALS) and spinal cord injury (SCI) (Clowry et al. 1991; Nijssen et al. 2017; Narasimhan 2006). However, in vitro production of spinal MNs and using MNs for drug discovery and disease modeling are hindered due to the inefficient MNs differentiation or inappropriate posterior identity.

Human pluripotent stem cells (hPSCs), including human embryonic stem cells (hESCs) and human induced pluripotent stem cells (hiPSCs), have the potential to generate various cell types in vitro and hold promise for disease modeling and cell-replacement therapies (Ebert and Svendsen 2010; Karagiannis et al. 2019; Thomson et al. 1998; Takahashi et al. 2007; Yu et al. 2007). Many motor neuron differentiation protocols have been developed over the past decades (Li et al. 2005; Lee et al. 2007; Li et al. 2008; Patani et al. 2011; Qu et al. 2014; Ben-Shushan et al. 2015; Du et al. 2015; Cutarelli et al. 2021; Hudish et al. 2020). Generally, hPSCs were firstly induced to form neuroepithelial (NE) cells at embryonic body (EB) or monolayer culture, subsequently specified to OLIG2 positive motor neuron progenitors (MNPs) under the activation of retinoic acid (RA) and sonic hedgehog (SHH). These procedures require 3-4 weeks to differentiate hPSCs into MNPs and another 1-2 weeks to differentiate MNPs into immature MNs, in total 8-10 weeks to generate mature MNs from hPSCs. Alternatively, hPSCs and human fibroblasts can be converted into MNs within 2-3 weeks by forcing the expression of MN inducing transcription factors (Hester et al. 2011; Son et al. 2011). Of note, these inductions of motor neurons from hPSCs predominantly produce cells of mixed hindbrain/cervical axial identities, but are inept in generating high numbers of more posterior thoracic/lumbosacral spinal cord motor neurons, which are in most cases of key targets of disease and injury.

Spinal motor neuron development initiates from gastrulation, when epiblast cells under dramatic proliferation, differentiation and migration to form three germ layers along the AP axis (Tam and Behringer 1997; Lu et al. 2001; Solnica-Krezel 2005). However, the mechanism of AP patterning during the development of the central nervous system (CNS) remains obscure. In vivo transplantation experiments of chick embryos revealed that the nodes exhibited disparate competency at different embryonic stages for posterior nervous system induction (Storey et al. 1992). Besides, evidence from

mutant T-box gene *Tbx6* in mouse embryos showed that *Tbx6* absent cells switched their cell fates from posterior somites into neuronal cells and formed three neural tube-like structures (Chapman and Papaioannou 1998). Cell lineage segregation study by clonal analysis in early mouse embryos further indicated that trunk neural ectoderm and neighboring mesoderm derivatives share a common progenitor, namely neuromesodermal progenitor (NMP) (Tzouanacou et al. 2009). NMPs are localized in the caudal lateral epiblasts (CLE) of E8.5 mouse embryos, and express both *Sox2* and *Brachyury (T)* (Henrique et al. 2015). Based on these developmental trajectories, mouse and human NMPs (hNMPs) were generated from mESCs and hPSCs and can be differentiated into neural and mesodermal cells in vitro (Turner et al. 2014; Gouti et al. 2014; Davis-Dusenbery et al. 2014; Wind et al. 2021; Wymeersch et al. 2021). The chromatin accessibility assay showed that the regionalization mechanism along the AP axis during neural induction supports the dual origin of CNS, i.e., the brain and posterior spinal cord are generated from distinct progenitor populations (Metzis et al. 2018). Methods have been established to derive spinal motor neurons through NMPs. For example, Verrier and colleagues established a protocol to rapidly and reproducibly induce human spinal cord progenitors from hNMPs-like cells, but these cells and their derivatives only expressed anterior spinal cord markers such as *HOXB4*, *HOXC6* and *HOXA7* (Verrier et al. 2018). A recent study also reported the generation of NMP-derived pre-neural progenitors (PNPs) which have the stem-cell like self-renew capacity and can be used to make neural crest progenitors with a posterior identity (Cooper et al. 2022). Moreover, transplantation of spinal cord neural stem cells derived from hPSCs through hNMP-stage showed functional recovery in SCI rat models (Kumamaru et al. 2018). Nevertheless, only about 50% of these hNMP-like cells expressed both SOX2 and Brachyury (T).

Thus, the establishment of high-purity human spinal cord neural progenitor cells (hSCNPCs) that are readily attainable for efficient differentiation of posterior spinal motor neurons remains unresolved.

In this study, we established a protocol to generate hSCNPCs from hPSCs through high-purity hNMPs. hSCNPCs showed molecular properties of spinal cord and were readily passaged up to 40 times in vitro. These hSCNPCs could be further differentiated into homogeneous spinal motor neurons, and exhibited posterior spinal cord identities. The spinal motor neurons after quick functional maturation could form neuromuscular junction (NMJ)-like structures when co-cultured with muscle fibers.

Xu *et al. Cell Regeneration*   (2023) 12:15

Page 3 of 21

Results

Generation and characterization of human spinal cord neural progenitor cells from hPSCs

To generate NPCs with spinal cord property and posterior regional identity from hPSCs, we mimicked the posterior spinal cord development in vitro by differentiating hPSCs into hSCNPCs through high-purity hNMPs (Fig. 1A). Feeder-free cultured hESCs were dissociated into single cells, seeded at 40,000 cells/cm^2 and maintained in mTeSR medium for 1 day to form small clusters, then differentiated in N2B27 medium containing dual-SMAD inhibitors, FGF2 and CHIR99021 for another 3 days. High-purity hNMPs with 90% efficiency were obtained at day 4 (D4) by detecting SOX2 and Brachyury (T) double positive cells (Fig. 1B and C). CDX2, another NMP marker was also highly expressed in hESCs-derived hNMPs (Fig. S1A). To further investigate the molecular profiles of hNMPs, we performed bulk RNA sequencing on samples collected on each day from D0 to D4 and compared our hNMPs with previously reported hNMPs, which were isolated by NKX1-2::GFP cell sorting (Verrier et al. 2018). Principal component analysis (PCA) demonstrated a clear differentiation trajectory from hESCs to hNMPs, and showed a high correlation between the D4-hNMPs with NKX1-2 enriched hNMPs (Fig. 1D), suggesting that this protocol represents a new route to NMP generation.

Next, high-purity hNMPs were subjected to hSC-NPCs differentiation. At D4, hNMPs were dissociated into single cells and re-plated with a seeding density of 100,000 cells/cm^2 in neural determination (NeuDet) medium, which contains dual-SMAD inhibitors, FGF2, FGF8, CHIR99021 and Compound E for another 6 days (Fig. 1A). Real-time quantitative PCR (RT-qPCR) analysis showed that the pluripotent gene *POU5F1* and hNMP marker gene *NKX1-2* were downregulated, while *CDX2* and neural progenitor marker genes *SOX2*, *PAX6* and *NKX6-1* and HOX family genes of posterior identity such as *HOXC9* and *HOXC10* were upregulated (Fig. S1D). By day 10 (D10), these hSCNPCs can be passaged in medium containing Purmorphamine,
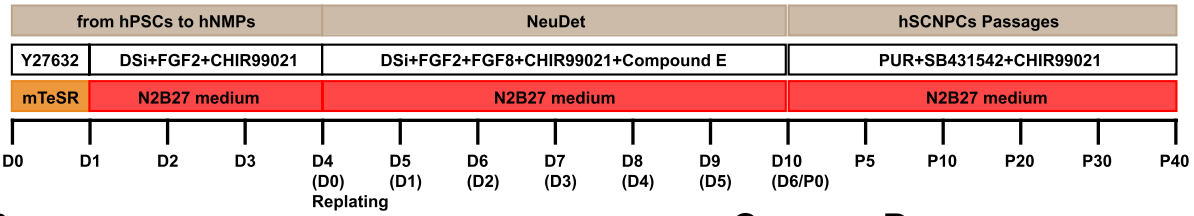
SB431542 and CHIR99021 over 40 times in vitro with normal karyotype (Fig. 1A, E and S1E). Immunofluorescent staining showed that hSCNPCs expressed high percentage of pan-NPC markers NESTIN, SOX1, SOX2 and PAX6 (Fig. 1F and G), as well as expressed moderate level of proliferation marker KI67 and spinal cord specific markers, such as NKX6-1 (~60%), NKX2-2 (~30%) and OLIG2 (~5%) (Fig. 1F and G). Human iPSCs can also be differentiated into spinal cord neural progenitor cells (hereafter referred to as hiSCNPCs) through neuromesodermal progenitor cells (hereafter referred to as hiNMPs) with the same protocol, indicating the robustness of this method (Figs. S1B, S1C and S1F).

To further determine the dynamic changes from hESCs to hSCNPCs at the transcriptomic level, we performed bulk RNA sequencing during NeuDet stage and hSCNPCs at different passages. PCA analysis based on regulon expression showed that three major cell groups, hNMPs, differentiating neural progenitors and passaged hSCNPCs, were aligned in a timely order (Fig. 1H). Regulon analysis showed that hNMPs mainly enriched with Gene Ontology (GO) terms of cell cycle process, Wnt signaling pathway and fibroblast growth factor receptor signaling pathway; NeuDet stage differentiating neural progenitors mainly enriched with stem cell differentiation and spinal cord development; passaged hSCNPCs enriched mainly with anterior/posterior pattern specification and neural precursor cell proliferation (Fig. 1I). Interestingly, we observed a caudalized shift of HOX genes expression from *HOXC6-8* at NeuDet stage to *HOXC9-10* in passaged hSCNPCs (Fig. 1I), suggesting an enhanced posterior signature during the derivation process. Comparison of the transcriptome of our hSCNPCs with that of human developing brain (Allen Brain Atlas) and human developing spinal cord (Rayon et al. 2021) confirmed that hSCN-PCs are resembling to human developing spinal cord (Fig. 1J).
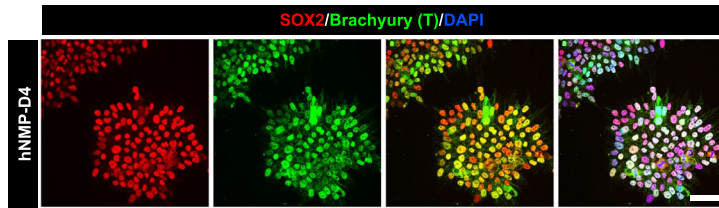
(See figure on next page.)

Fig. 1 Generation and characterization of human spinal cord neural progenitor cells from hPSCs. **A** Schematic procedure for generating hSCNPCs and hiSCNPCs from hPSCs (H9, DC60-3, DC87-3) with all stages, media and factors. DSi represents dual-SMAD inhibitors SB431542 and Dorsomorphin. **B** Immunostaining of hNMPs markers SOX2 and Brachyury (T) at day 4. Scale bar, 50 μm. **C** Quantification of SOX2 and Brachyury (T) double positive cells over DAPI of hNMPs-D4. *n* = 4 independent experiments. Data are represented as mean ± SD. **D** Principal component analysis of time course samples during hNMPs differentiation and the previously published samples of NKX1-2-GFP sorted human nmps (Verrier et al. 2018). **E** Cumulative growth curve of hSCNPCs counts over 40 passages. n = 4 independent experiments. Data are represented as mean ± SD. **F** Immunostaining of hSCNPCs (top panel exhibited pan-NPC markers and proliferation marker; bottom panel exhibited spinal cord specific NPC markers). Scale bar, 50 μm. **G** Quantification of results shown in Fig. 1F. *n* = 5 independent experiments. Data are represented as mean ± SD. **H** Principal component analysis of samples from hESCs (H9) to hSCNPCs at each time point shown in Fig. 1A. **I** The heat-map showing three regulon groups in samples of hESCs (H9) to hSCNPCs with listing representative regulon transcription factors (numbers of predicted target genes by SCENIC in the brackets) and enriched GO terms for each regulon group. **J** Comparative analysis of whole transcriptome of hSCNPCs at different passages to dataset from Allen Brain Atlas of developing human brain and previous published dataset of developing human spinal cord
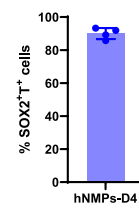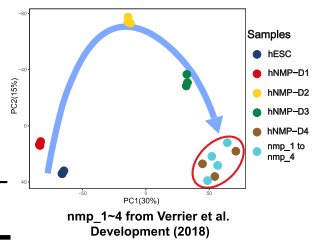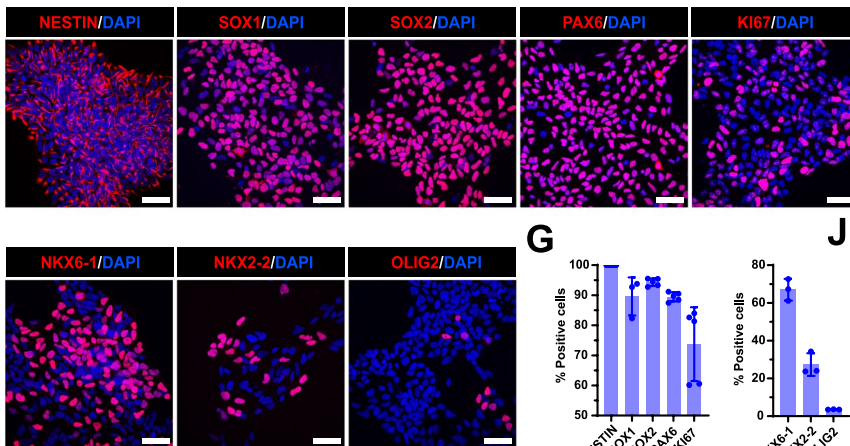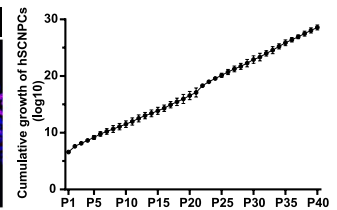
Xu *et al. Cell Regeneration*   (2023) 12:15

Page 4 of 21

Fig. 1 (See legend on previous page.)

Xu *et al. Cell Regeneration*   (2023) 12:15

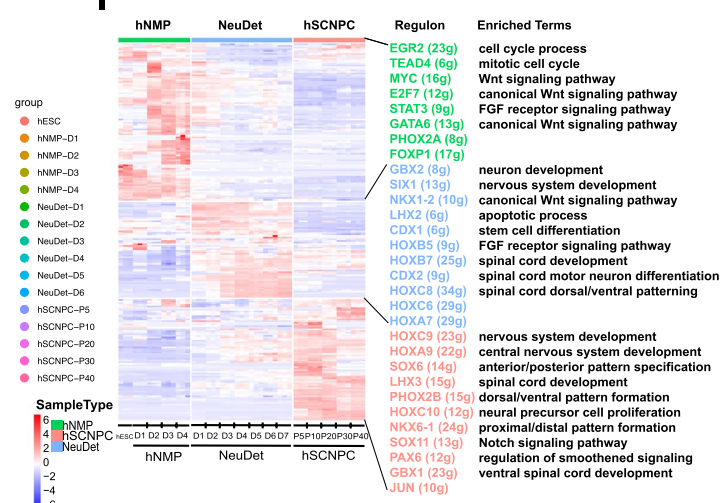Page 5 of 21
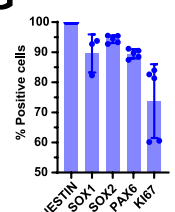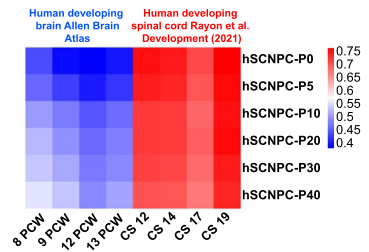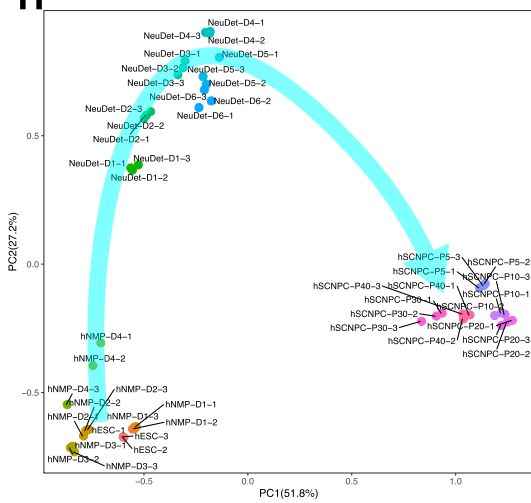
Taken together, these results suggest that we have successfully obtained a neural progenitor cell line with human spinal cord features.

Fast and direct differentiation of posterior spinal motor neurons from hSCNPCs

To test the motor neuron differentiation ability of hSC-NPCs, we dissociated hSCNPCs into single cells and seeded with a density of 100,000 cell/cm^2 on PDL and Matrigel-coated plates and differentiated in N2B27 medium containing Purmorphamine, Compound E, brain-derived neurotrophic factor (BDNF), glial cell line-derived neurotrophic factor (GDNF) and Neu-rotrophin-3 (NT-3) (Fig. 2A). In this medium, hSCN-PCs can be quickly differentiated into immature motor neurons expressed markers of HB9 ($\sim$90%) and ISL1 ($\sim$70%) at day 6 (D6) (Fig. 2B and D). By day 18 (D18), hSCNPCs-derived motor neurons expressed homogeneously mature neuronal markers, such as SMI-32 ($\sim$90%), NEUN ($\sim$90%) and MAP2 ($\sim$90%) (Fig. 2C and D). These cells also expressed motor neuron subtype-specific markers, such as choline acetyltransferase (ChAT) and vesicular acetylcholine transporter (VAChT) at high percentages (Fig. 2E and F). Other neuronal subtypes, such as glutamatergic neurons (VGLUT), GABAergic neurons (GAD67) and dopaminergic neurons (TH), were barely detectable (Fig. 2E and F), suggesting that this method is a highly efficient spinal motor neuron differentiation protocol.

HOX genes play an important role in the rostrocaudal axis and spinal cord patterning, immunostaining analysis showed that hSCNPCs-derived spinal motor neurons mainly expressed HOXC9 ($\sim$70%) and HOXD11 ($\sim$30%), which were associated with thoracic and lumbar spinal domains, respectively (Fig. 2G and H). The regional identities of hindbrain (HOXB4), cervical spinal (HOXC6) and lumbar spinal cord (HOXD10) were hardly detectable (Fig. 2G and H). To confirm the spinal motor neurons with posterior identities, we performed double staining of motor neuron marker (SMI-32) and posterior marker (HOXC9). The double staining results showed that $\sim$61.53% SMI-32$^+$/HOXC9$^+$ cells were detected as

posterior spinal motor neurons (Figs. S3E and S3F). To further illustrate the expression patterns of *HOX* family genes during spinal motor neuron differentiation, we profiled 4 *HOX* clusters of 39 genes in the RNA-seq data. In line with the immunostaining results, spinal motor neurons generated from hSCNPCs specifically expressed *HOXC9* (Fig. 2J). Together, these results suggest that the motor neurons this protocol induced are the posterior spinal motor neurons.

Similarly, the motor neurons derived from hiPSCs through hiSCNPCs using the same protocol also showed comparable expression levels of spinal motor neuron markers and HOX proteins (Fig. S2B). Both hESCs-derived hSCNPCs and hiPSCs-derived hiSCNPCs can be passaged in vitro up to 40 times (Fig. 1E). To test whether the expandable stage hSCNPCs still can be differentiated into posterior spinal motor neurons, we differentiated hSCNPCs at P40 and performed immunofluorescent staining of neuronal markers (TUJ1/NEUN/HB9/SMI-32/ChAT/VAChT/ISL1) and posterior marker (HOXC9). The results showed that, hSCNPCs at P40 can still be efficiently differentiated into spinal motor neurons with posterior identities (Figs. S4A-S4D).

To gain insights into the transcriptomic alterations during spinal motor neuron differentiation, we employed time course RNA-seq analysis every 6 days from D0 to D30, as well as D42. The SCENIC algorithm identified 252 regulons (Fig. S2C) and the PCA analysis showed a turning point at D6 (Fig. 2I). Heatmap and GO term analysis showed that D0-D6 regulons were enriched with terms of spinal cord patterning, cell cycle DNA replication and neural precursor cell proliferation, and regulons of late stage were corresponding to neuron migration, neural tube formation, neuromuscular junction development and neurotransmitter secretion (Fig. S2C). Hence, the spinal motor neuron differentiation process could be divided into two major events: motor neuron differentiation and maturation. We observed temporal activation of transcription factors that may account for the cell fate transition of hSCNPCs, for example, *JUN*, *GBX2*, *FOXP2*, *ONCUT3* and *SIX3* (Fig. S2C). We also confirmed by RT-qPCR that the expression of NPC marker genes *NESTIN*

(See figure on next page.)

Fig. 2 Fast and high-efficient posterior spinal cord motor neuron differentiation from hSCNPCs. **A** Schematic illustration of direct spinal motor neurons differentiation from hSCNPCs and hiSCNPCs (derived from H9, DC60-3 and DC87-3). **B** Immunofluorescent images demonstrating the expression of motor neuron markers HB9, ISL1 of hSCNPCs direct differentiated spinal motor neurons at day 6. Scale bar, 50 μm. **C** Immunofluorescent images demonstrating the expression of mature motor neuron marker SMI-32 and mature neuronal markers NEUN and MAP2 of hSCNPCs direct differentiated spinal motor neurons at day 18. Scale bar, 50 μm. **D** Quantification of results shown in Fig. 2B and C. n = 5 independent experiments. Data are represented as mean ± SD. **E** Immunofluorescent images of neurotransmitter markers ChAT, VAChT, VGLUT, GAD67 and TH of hSCNPCs-derived spinal motor neurons at day 18. Scale bar, 50 μm. **F** Quantification of results shown in Fig. 2E. n = 5 independent experiments. Data are represented as mean ± SD. **G** Immunofluorescent staining of HOX family genes HOXB4, HOXC6, HOXC9, HOXD10 and HOXD11 of hSCNPCs-derived spinal motor neurons at day 18. Scale bar, 50 μm. **H** Quantification of results shown in Fig. 2F. n = 5 independent experiments. Data are represented as mean ± SD. **I** Principal component analysis of samples from hSCNPCs to spinal motor neurons at each time point shown in Fig. 2A. **J** 39 HOX genes expression profiles during spinal motor neuron differentiation from hSCNPCs
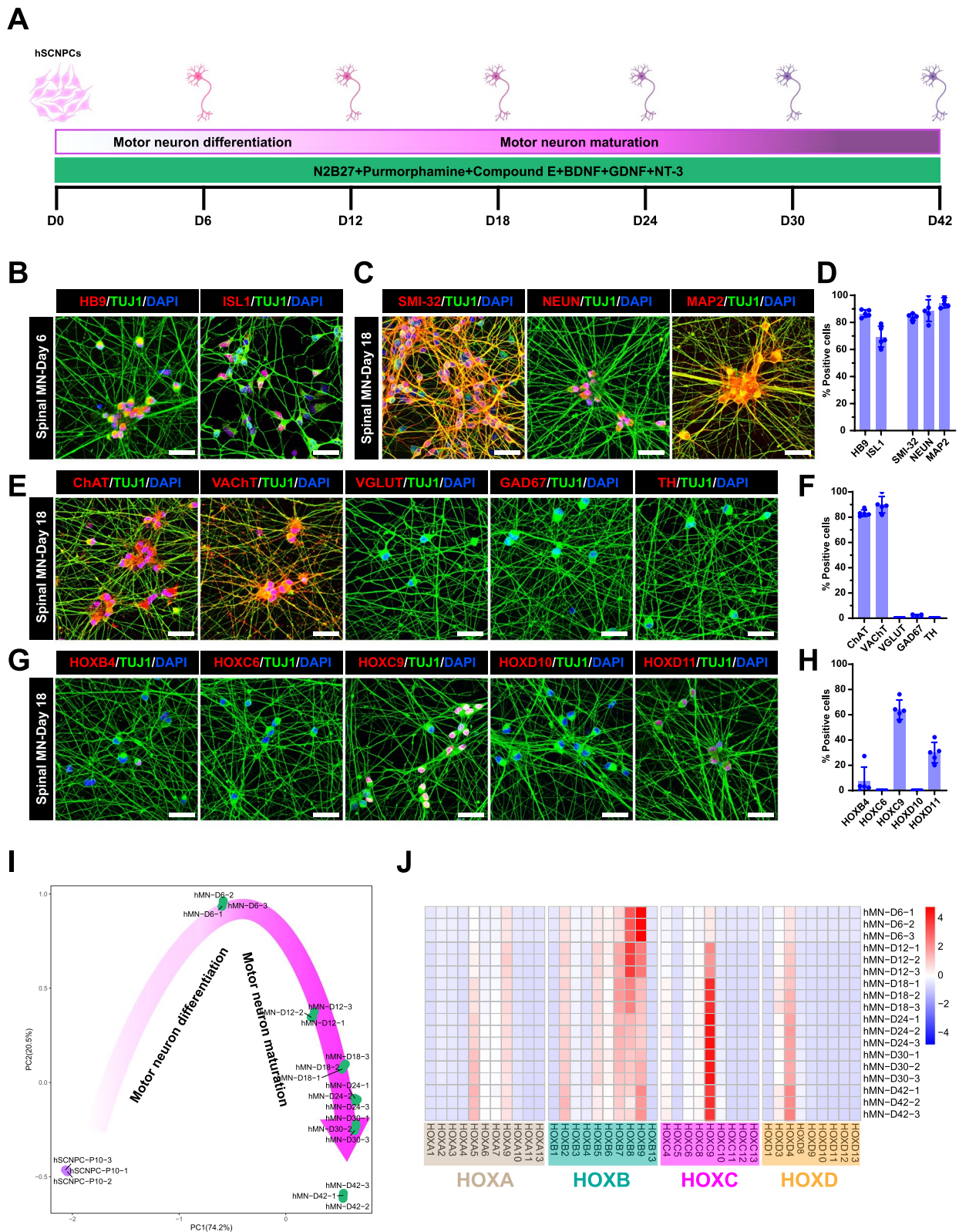
Xu *et al. Cell Regeneration*   (2023) 12:15

Page 6 of 21

Fig. 2 (See legend on previous page.)

Xu *et al. Cell Regeneration*   (2023) 12:15

Page 7 of 21

and *NKX2-2* were downregulated, while motor neuron progenitor specific marker *NKX6-1* increased from D0 to D18 and remained the expression level thereafter, indicating that *NKX6-1* may play an important role during motor neuron fate determination and maintenance; the expression of immature neuronal marker *TUJ1* increased sharply from D0 to D6, then dramatically decreased and maintained a relatively low level; and immature motor neuron markers *HB9* and *ISL1* increased from D0 to D12 then slowly decreased (Fig. S2A). In contrast, the expression of mature neuronal marker *NEUN* and mature motor neuron markers *ChAT* and *VAChT* increased from D0 to D12, and were maintained afterwards (Fig. S2A).

To test whether hSCNPCs have the potential to give rise to other cell types of the spinal cord, we applied a spontaneous differentiation system to hSCNPCs. hSC-NPCs were plated as single cells and differentiated in N2B27 medium without additional patterning factors. In this condition, hSCNPCs differentiated into mature neurons with centimeter-long axon bundles (Figs. S3A and S3B). MicroRNA-218 (mir-218) was previously reported as an authentic marker of both rodent and human motor neurons (Amin et al. 2015; Hoye et al. 2018; Reichenstein et al. 2019; Amin et al. 2021). To compare the difference between spinal motor neurons and spontaneous differentiated neurons, time course RT-qPCR was performed for samples from both systems every 3 days from D0 to D21. The results showed that *mir-218-2* was specifically elevated in cells from spinal motor neuron differentiation system (Fig. S3C). Albeit the much lower efficiency of motor neuron differentiation, we still detected HB9 positive cells in spontaneous culture. Interestingly, interneuron markers GABA and Somatostatin (SST) and astrocyte marker S100β were also presented in spontaneous differentiation (Fig. S3D), indicating that hSCNPCs

as neural progenitors have the capacity to generate the major neural cell lineages of spinal cord.

Functional characterization of posterior spinal motor neurons derived from hSCNPCs

To characterize the functional maturation of the posterior spinal motor neurons, we performed whole-cell patch-clamp and CMOS-based high-density microelectrode array (HD-MEA) recordings. Spinal motor neurons co-cultured with astrocytes exhibited a mature morphology with abundant dendrites and long axons, and expressed mature motor neuron marker SMI-32 (Figs. S5A and S5B). The action potentials (APs) were examined during 42 days of spinal motor neuron differentiation by whole-cell patch-clamp (Fig. 3A). In response to a series of step current injections, 20% neurons could quickly generate single spike at D6 of differentiation and the mean amplitude was 24.12 ± 6.39 mV. After 12 days of differentiation, 50% neurons fired trains of APs and the mean amplitude was 41.27 ± 3.53 mV. At day 18, near 80% neurons fired repetitive APs at a mean amplitude of 47.76 ± 3.27 mV. As maturation progressively increased, 100% of recorded neurons showed sharp and repetitive spikes at 24 days, 30 days and 42 days of differentiation with mean amplitudes of 67.77 ± 2.69 mV, 71.91 ± 2.52 mV and 69.14 ± 2.63 mV, respectively (Fig. 3A-C and S5C). Statistical analysis of AP thresholds and resting membrane potentials (RMPs) showed that the mean values of AP thresholds and RMPs became more negative as the in vitro culture proceeded and reached a plateau after 24 days of spinal motor neuron differentiation at -32.15 ± 1.14 mV and -48.73 ± 1.12 mV, respectively (Fig. 3D and E). A gradual reduction from ~1 GΩ to ~0.5 GΩ of input resistance (Rin) was also observed during spinal motor neuron maturation (Fig. 3F). The F-I

(See figure on next page.)

Fig. 3 Functional characterization of hSCNPCs direct differentiated posterior spinal motor neurons. **A** Representative recording traces of hSCNPCs-derived spinal motor neurons from day 6 to day 42 in response to step current injection. **B** Percentages of hSCNPCs-derived spinal motor neurons from day 6 to day 42 with AP and no AP. N numbers of technical replicates were shown in figures from 3 independent experiments. Data are represented as mean ± SD. **C** Quantification of AP amplitude of hSCNPCs-derived spinal motor neurons from day 6 to day 42. N numbers of technical replicates were shown in figures from 3 independent experiments. Data are represented as mean ± SD. **D** Quantification of AP threshold during hSCNPCs spinal motor neurons differentiation from day 6 to day 42. N numbers of technical replicates were shown in figures from 3 independent experiments. Data are represented as mean ± SD. **E** Quantification of resting membrane potential (RMP) of hSCNPCs-derived spinal motor neurons from day 6 to day 42. N numbers of technical replicates were shown in figures from 3 independent experiments. Data are represented as mean ± SD. **F** Quantification of input resistance (Rin) of hSCNPCs-derived spinal motor neurons decreased over the differentiation process. N numbers of technical replicates were shown in figures from 3 independent experiments. Data are represented as mean ± SD. **G** Comparison of F-I curves from hSCNPCs-derived spinal motor neurons at day 6, day 12, day 18, day 24, day30 and day 42. Data were collected from 3 independent experiments. Data are represented as mean ± SD. **H** Spatial distribution maps of active spikes and the quantification results during spinal motor neuron differentiation from day 6 to day 42. $n = 3$ independent experiments. Data are represented as mean ± SD. **I** Representative mean firing rate and the quantification results during spinal motor neuron differentiation from day 6 to day 42. $n = 3$ independent experiments. Data are represented as mean ± SD. **J** Representative axon tracking maps during spinal motor neuron differentiation from day 6 to day 42. **K** Quantification results of axon tracking during spinal motor neuron differentiation from day 6 to day 42. Data were collected from 3 independent experiments. Data are represented as mean ± SD. **L** Network analysis during spinal motor neuron differentiation from day 6 to day 42 and cortical neuron at day 18 as a positive control. **M** Immunostaining of pre- (SYP, Synaptophysin) and post-synaptic (PSD95) markers of hSCNPCs-MNs and cortical neurons at day 18. Scale bar, 50 μm
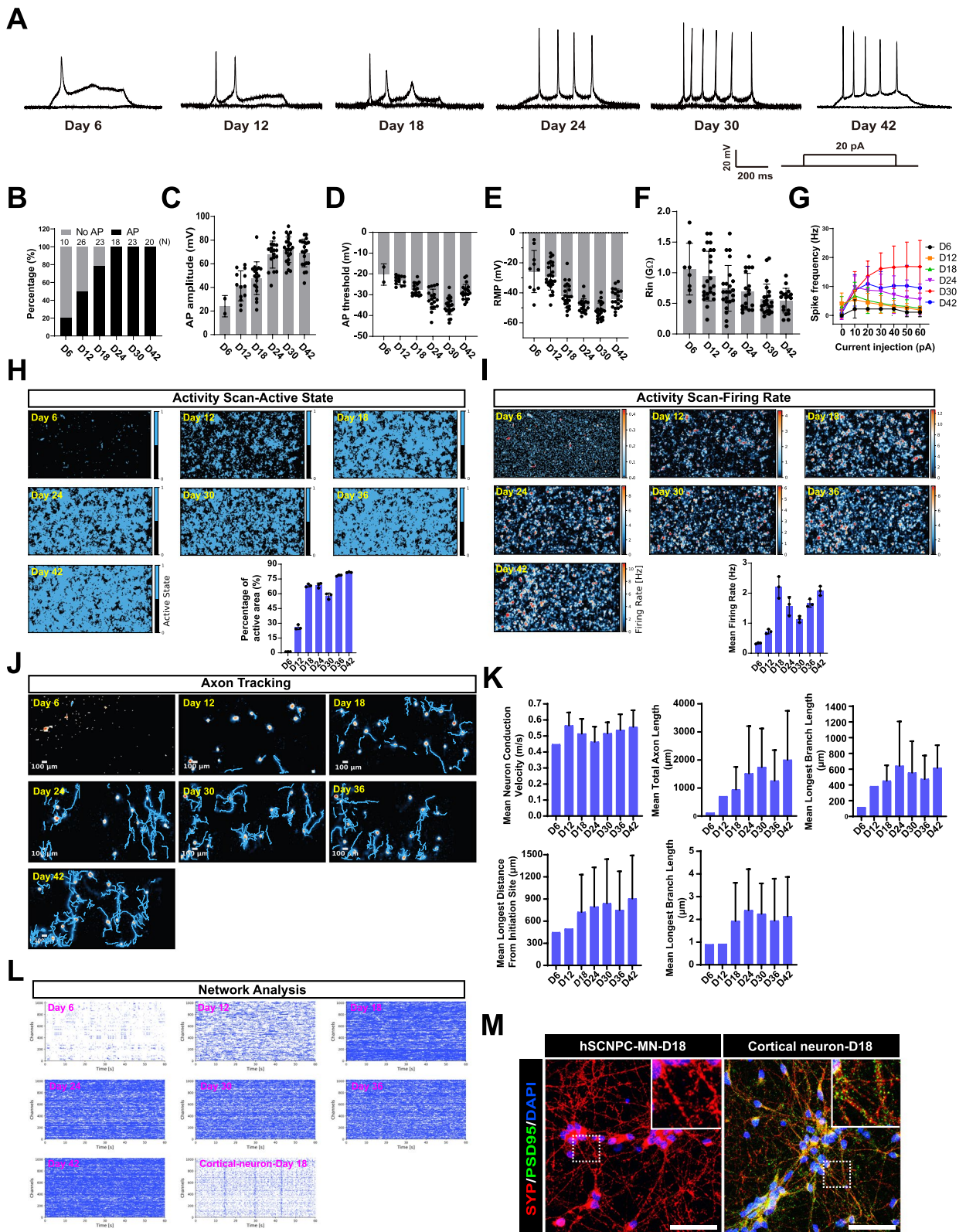
Fig. 3 (See legend on previous page.)

Xu *et al. Cell Regeneration*   (2023) 12:15

Page 9 of 21

curves of spinal motor neurons from D6 to D42 exhibited a gradual increase in spike frequency under the increasing current injections from 0 pA to 30 pA and reached a plateau under the current injection over 30 pA (Fig. 3G). Together, whole-cell patch-clamp recordings reveal that hSCNPCs-derived spinal motor neurons exhibit a fast maturation property at 24 days of differentiation, and show the highest electrophysiological function at D30 and then under a slight degeneration at D42 of differentiation.

To comprehensively investigate the maturity of spinal motor neurons, we utilized the CMOS-based HD-MEA platform, which is a high-throughput and high-resolution system containing 26,400 electrodes and 1024 simultaneous recording channels (Muller et al. 2015; Yuan et al. 2020; Sundberg et al. 2021). We first scanned and analyzed the entire HD-MEA electrode array to examine spontaneous neural activities during spinal motor neuron differentiation. The percentage of active electrodes rose rapidly from D6 to D18 and then was stabilized at about 75% thereafter (Fig. 3H). The presented heatmaps of firing rate over the time course differentiation from D6 to D42, and statistical analysis of mean firing rate (MRF) showed that the time span for functional maturity is from D18 to D42, which is consistent with whole-cell patch-clamp results (Fig. 3C and I). Then, axon tracking and spike sorting assays were performed to depict the functional images of axons and neurites of single neurons during spinal motor neuron differentiation (Fig. 3J). We assessed the axon tracking metrics including mean neuron conduction velocity (m/s), mean total axon length (μm), mean longest branch length (μm), mean longest distance from initiation site (μm) and mean longest latency (ms). These results showed that all of the parameters described above were steadily increased accompanying the differentiation progresses, pointing to a step-wise electrophysiological maturation of the spinal motor neurons (Fig. 3K).

Neural networks or neural circuits are featured by synchronous signals which are based on connections between pre- and postsynaptic neurons. To assess the neural network properties of spinal motor neurons, we performed network analysis during differentiation. No synchronous burst was observed from D6 to D42 after differentiation, while network oscillations were demonstrated in cortical neurons differentiated from iNSCs previously generated in our lab (Zhang et al. 2019) (Fig. 3L). Moreover, we also used whole-cell patch-clamp to record spontaneous postsynaptic currents (sPSC) of spinal motor neurons at D30 of differentiation and no sPSC were recorded (Fig. S5D). Although the spinal motor neurons can produce robust and abundant single burst (data not shown), they were yet to form microcircuit assembly under an in vitro culture system. We reasoned that the spinal motor neurons derived from hSCNPCs are of high purity and were not able to form synapses without other cell types. To test this hypothesis, immunofluorescent staining of pre- and postsynaptic markers synaptophysin (SYP) and PSD95 was performed to characterize synapse formation. The results showed that hSCNPCs-derived spinal motor neurons expressed only presynaptic marker synaptophysin but not postsynaptic marker PSD95, while iNSCs differentiated cortical neurons expressed them both (Fig. 3M).

Taken together, both whole-cell patch-clamp and CMOS-based HD-MEA results reveal that hSCNPCs differentiated spinal motor neurons exhibit a fast mature property from D18 onward.

Generation and characterization of 3D spinal motor neuron spheroids from hSCNPCs

Spinal motor neurons aggregate to form motor columns and pools in the spinal cord during vertebrate development, of which the somata reside in the spinal cord while the axons extend out to target muscles (Guthrie 2004; Dasen et al. 2005; De Marco Garcia and Jessell 2008). In order to mimic in vivo spinal motor neuron aggregates and neuron-muscle interaction in vitro, we generated three-dimensional (3D) spinal motor neuron spheroids from hSCNPCs and tried to find the suitable conditions for co-culture spinal motor neurons with muscle cells. Single hSCNPCs suspension was prepared and seeded in V-bottom 96-well plates at 50,000 cells/well to differentiate into 3D spinal motor neuron spheroids in the presence of Purmorphamine, Compound E, BDNF, GDNF, NT-3 and CultureOne™ supplement in N2B27 medium

(See figure on next page.)

Fig. 4 Three-dimensional spinal motor neuron spheroids differentiation from hSCNPCs. **A** Schematic illustration of the differentiation process of three-dimensional spinal motor neuron spheroids. **B** Fold changes of marker genes expression (relative to the expression level of GAPDH) during 3D spinal motor neuron spheroids differentiation. n = 4 independent experiments. Data are represented as mean ± SD. **C** Immunofluorescent staining of HB9, SMI-32 and NEUN in spinal motor neuron spheroids at day 12 after differentiation. Scale bar, 50 μm. **D** Immunofluorescent staining of MAP2, ChAT and VAChT in spinal motor neuron spheroids at day 12 after differentiation. Scale bar, 50 μm. **E** Immunofluorescent staining of HOXB4 and HOXC9 in spinal motor neuron spheroids at day 12 after differentiation. Scale bar, 50 μm. **F** Statistic analysis and quantification of Fig. 4E. n = 3 independent experiments. Data are represented as mean ± SD. Student's t test. *P* value was presented in the fig. **G** Statistical analysis of the efficiency of HB9 positive cells in 2D and 3D culture system. Data are represented as mean ± SD. Student's t-test, ns = not significant. **H** Statistical analysis of the efficiency of HOXC9 positive cells in 2D and 3D culture system. Data are represented as mean ± SD. Student's t-test, ns = not significant

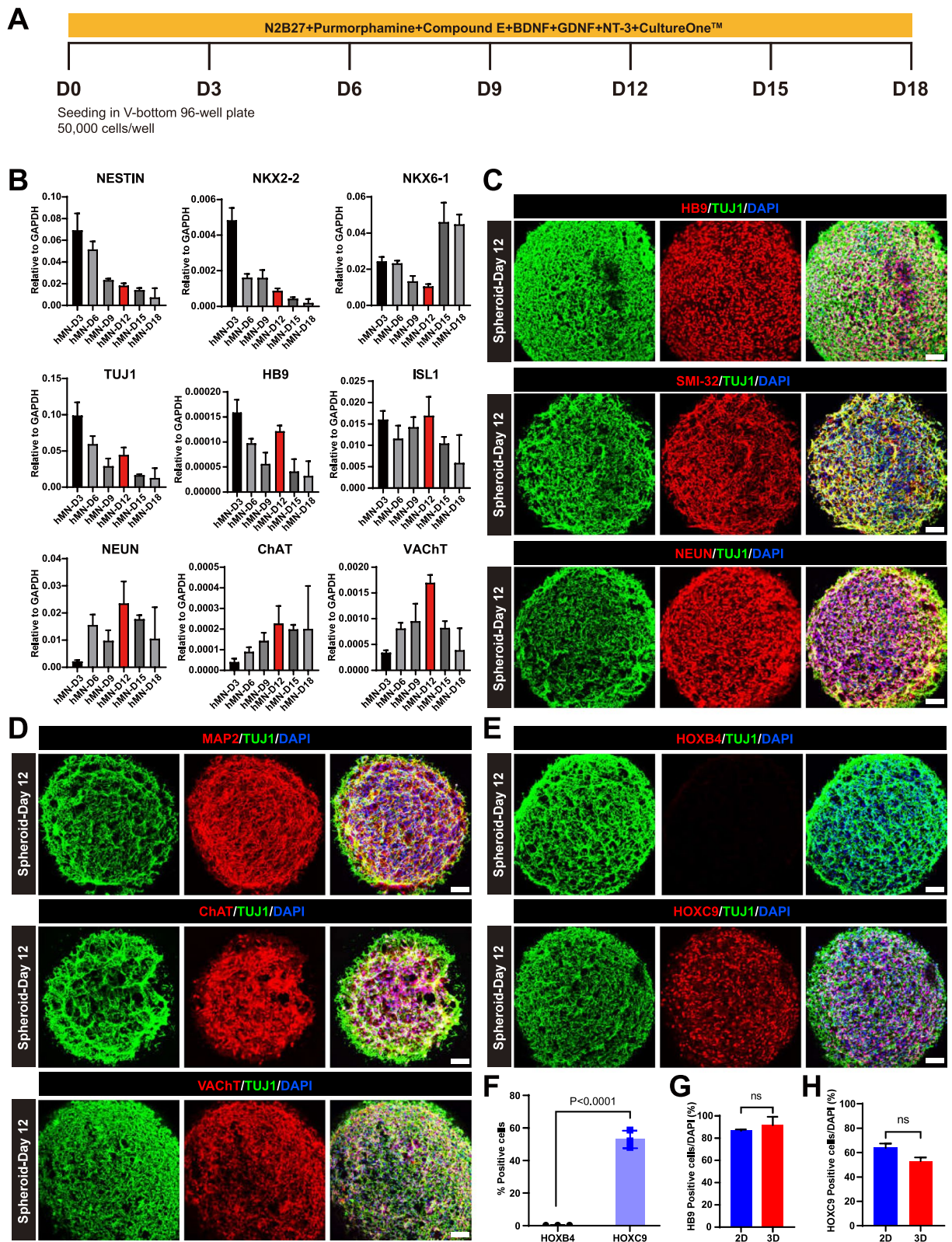Xu *et al. Cell Regeneration*　　(2023) 12:15

Page 10 of 21

Fig. 4 (See legend on previous page.)

Xu *et al. Cell Regeneration*   (2023) 12:15

Page 11 of 21

(Fig. 4A). Time course RT-qPCR showed that the expression levels of spinal cord neural progenitor marker genes *NESTIN*, *NKX2-2* and immature motor neuron marker genes *TUJ1*, *HB9* and *ISL1* declined in this 3D differentiation system; on the contrary, the expression of mature spinal motor neuron marker genes *NEUN*, *ChAT* and *VAChT* gradually increased until D12 (Fig. 4B). To further confirm the spinal motor neuron feature, maturity and regional identity of 3D spinal motor neuron spheroids at D12 of differentiation, we performed immunofluorescent staining of cryosection spheroids at D12. The results showed that hSCNPCs-derived 3D spinal motor neuron spheroids homogeneously expressed motor neuron markers HB9 and SMI-32, mature neuronal markers NEUN and MAP2 and mature motor neuron markers ChAT and VAChT (Fig. 4C and D). For regional identity, many cells (~60%) of spinal motor neuron spheroids expressed HOXC9, but no cell expressed HOXB4 (Fig. 4E and F). To compare the posterior motor neuron differentiation efficiency between 2D system and 3D system, we quantified the expression efficiency of motor neuron marker (HB9) and posterior marker (HOXC9) in 3D system and compared with the efficiency in 2D system. The statistical analysis showed that the efficiency of posterior motor neuron differentiation is similar between 2D and 3D system (Fig. 4G and H).

Collectively, these results suggest that the suitable time for spinal motor neuron spheroids to co-culture with muscle cells is at differentiation D12.

Formation pattern of complex and pretzel-shaped acetylcholine receptor aggregates during C2C12 myogenic differentiation

One of the most important roles of spinal motor neurons is to form neuromuscular junctions (NMJs) with targeted muscles, leading to muscle innervation. To model NMJ formation in vitro with hSCNPCs-derived spinal motor neurons, a robust and reproducible co-culture system of spinal motor neurons and skeletal muscles is a prerequisite. To obtain an optimized myotube differentiation condition, we tested four combinations of different cell seeding densities and durations of propagation stage, then differentiated the cells for another 6 days (Fig. S6A). Immunofluorescent staining of mature muscle fiber marker myosin heavy chain (MyHC) and fluorescent α-bungarotoxin (α-BTX) staining showed that C2C12 cells differentiated into the most complex structure and the highest numbers of AChR clusters with an initial seeding density of 40,000 cells/cm^2 and 2 days propagation (Figs. S6B and S6C). Thus, we established a differentiation protocol to proliferate C2C12 cells in propagation medium containing 10% FBS-DMEM for 2 days and subjected these cells to differentiate for 14 days with 2% horse serum (HS) (Fig. 5A). Immunostaining analysis showed that AChR accumulated into small plaques at day 4 of myogenic differentiation, which became branched forms and pretzel-like shaped clusters at day 6, and then diffused along the myotubes at day 8 (Figs. 5B and S6C). We also quantified the fiber length, fiber width, nuclei numbers per fiber, MyHC surface area, AChR area and the ratio of AChR to MyHC. The results showed that C2C12 fused into myotube and gradually matured to form muscle fibers from day 0 to day 6, and then degenerated afterwards (Fig. 5C).

Taken together, we have established a protocol to differentiate C2C12 into mature muscle fibers with abundant and pretzel-shaped aneural AChR clusters.

Co-culture spinal motor neuron spheroids and C2C12-derived muscle fibers to form NMJ-like structures in vitro

After obtaining the proper differentiation conditions for muscle cells and spinal motor neuron spheroids, we next sought to find a suitable condition to co-culture these two types of cells to model the NMJ formation in vitro. To this end, we first attempted to determine the co-culture medium by testing different combinations of basal medium (DMEM or N2B27), chemical additives (with or without supplementation of Purmorphamine and Compound E (P/E)) and serum (horse serum (HS) or Ultroser™ G serum substitute (UG)). Having separately cultured these two types of cells in these different co-culture media for 2 days, we found that 0.2% UG and DMEM medium supported both 3D spinal motor neuron spheroids differentiation and C2C12 myotube fusion more efficiently than the other conditions, and Purmorphamine or Compound E showed no additive effect (Fig. 6A and B). Furthermore, RT-qPCR confirmed that mature motor neuron marker genes *NEUN*, *VAChT* and *ChAT* and AChR associated markers *musk*, *chrng* and *chrne* were highly expressed in this condition (Fig. 6C and D). Hence, we have obtained a co-culture medium that facilitates both motor neuron and myogenic differentiation.

To co-culture motor neurons and muscle cells, we added differentiation day 12 spinal motor neuron spheroids onto day 4 muscle fibers derived from C2C12 myogenic differentiation, then cultured them in the DMEM medium supplemented with 0.2% UG for 2 days (Fig. 6E). Immunostaining analysis showed that spinal motor neuron spheroids extended neurites following the orientations of muscle fibers (Fig. 6F), indicating that muscle fibers may have a guiding cue on axonal growth of motor neurons. Furthermore, MyHC, TUJ1 and α-BTX co-staining showed that NMJ-like structures were formed in vitro after co-culturing hSCNPCs-derived 3D spinal

Xu *et al. Cell Regeneration*   (2023) 12:15
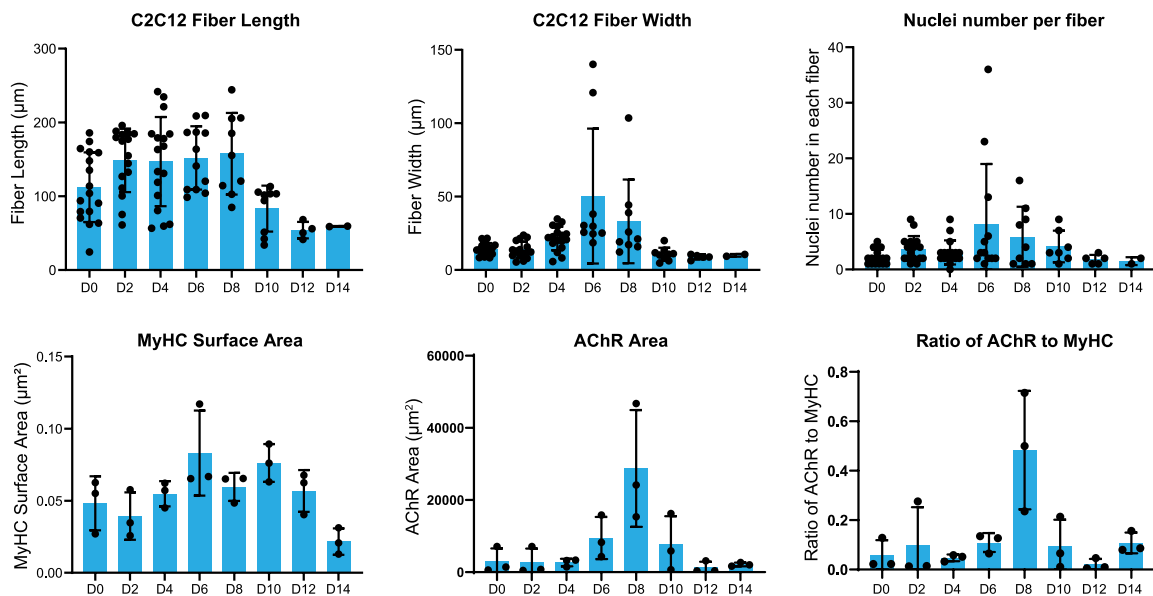
Page 12 of 21
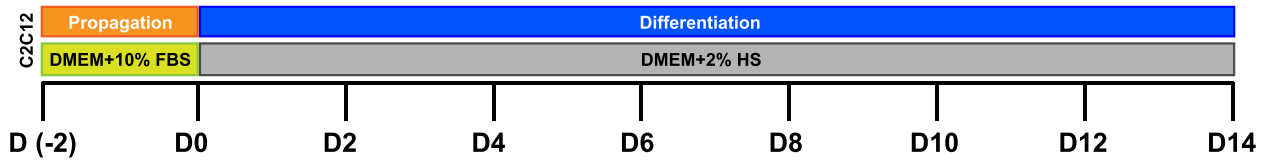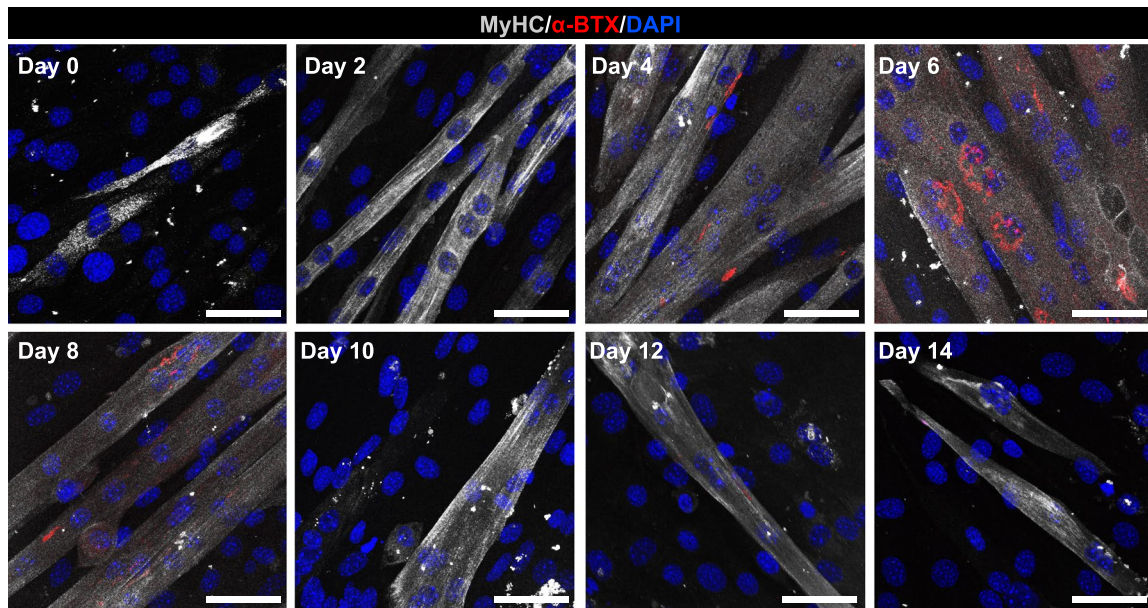
Fig. 5 Step-wise myogenic differentiation of C2C12. **A** Schematic procedure of C2C12 differentiation. **B** Immunostaining of muscle fiber marker (MyHC) and AChR during muscle fiber differentiation of C2C12 from day 0 to day 14. Scale bar, 50 μm. **C** Quantification results of Fig. 5B. Data were collected from 3 independent experiments. Data are represented as mean ± SD
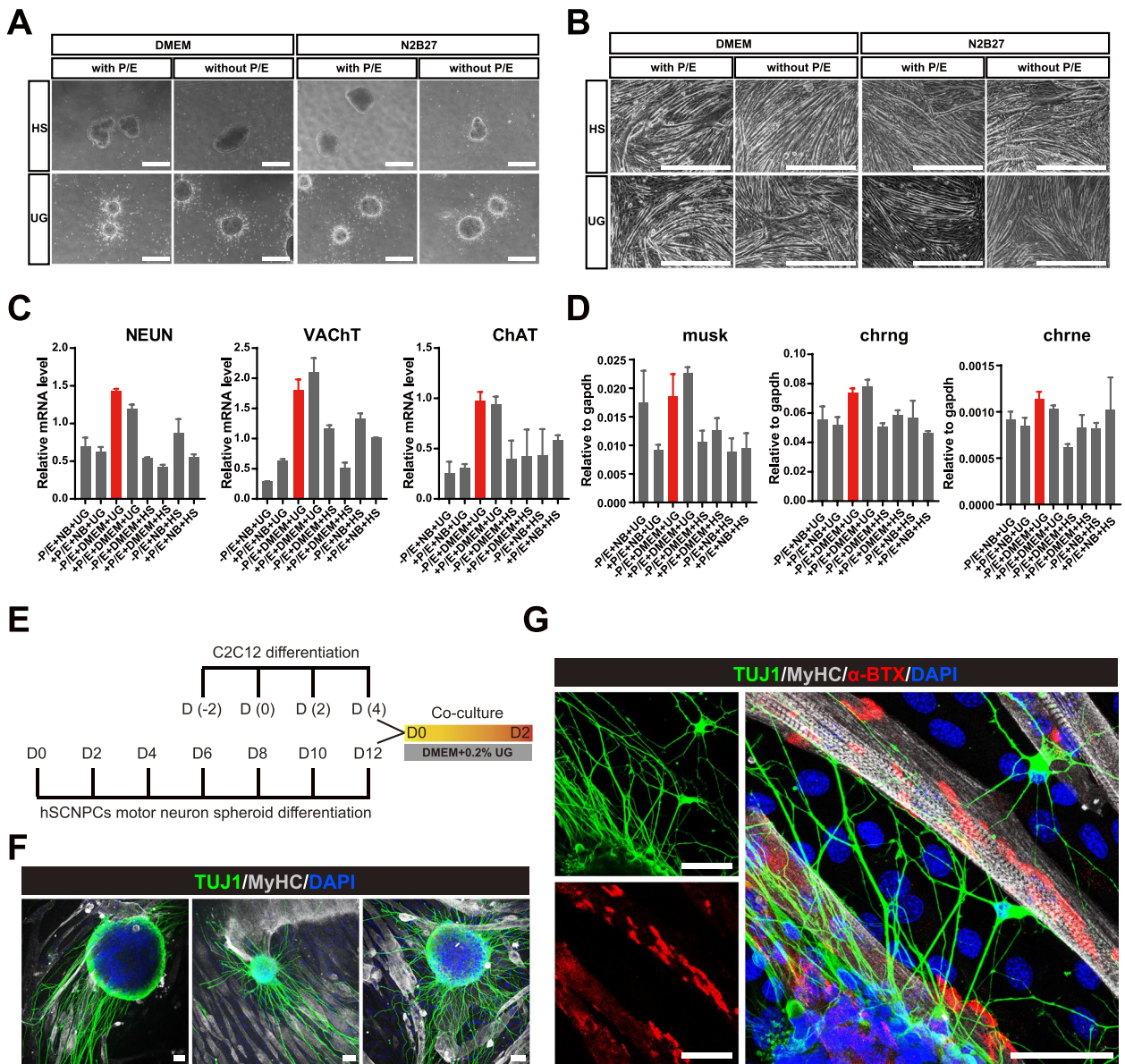
Xu *et al. Cell Regeneration*   (2023) 12:15

Page 13 of 21

Fig. 6 Co-culture of hSCNPCs-derived spinal motor neuron spheroids and C2C12-derived muscle fibers to form neuromuscular junctions in vitro. **A** Representative bright-field images of the differentiated spinal motor neuron spheroids based on differential co-culture medium compositions. Scale bar, 100 µm. **B** Representative bright-field images of the differentiated muscle fibers based on differential co-culture medium compositions. Scale bar, 100 µm. **C** Fold changes of mature motor neuron marker genes (NEUN, ChAT and VAChT) expression on differential co-culture medium. Data were collected from 2 independent experiments. Data are represented as mean ± SD. **D** Fold changes of AChR markers (musk, chrng and chrne) genes expression on differential co-culture medium. Data were collected from 2 independent experiments. Data are represented as mean ± SD. **E** Schematic illustration of co-culture model. **F** Immunofluorescent images demonstrating motor neurons extending patterns when co-cultured with muscle fibers. Scale bar, 50 µm. **G** Immunofluorescent staining of neuronal marker (TUJ1), mature muscle marker (MyHC) and AChR marker (α-BTX) on co-cultured cells. Scale bar, 50 µm

motor neuron spheroids with C2C12-derived muscle fibers for 2 days (Fig. 6G).

Taken together, we have established a co-culture system, in which both spinal motor neurons and muscle cells could differentiate to maturation and form NMJ-like structures in vitro.

Discussion

In this study, we differentiated hPSCs into self-renewal hSCNPCs through hNMPs. These neural progenitor cells express homogeneous pan-NPC markers as well as spinal cord specific markers and can be passaged over 40 times in vitro. The hSCNPCs could be further differentiated

into high-purity motor neurons with posterior spinal cord regional identity. The spinal motor neurons derived from hSCNPCs could be electrophysiologically mature after long-term differentiation. Moreover, co-culture of hSCNPCs-derived spinal motor neurons with C2C12-derived muscle fibers could form NMJ-like structures in vitro.

There is enormously regional diversity in the central nervous system. Conventionally, the generation of regional specific NPCs from hPSCs follows a general principle of neural development, hypothesized as an "activation transformation" paradigm. This model proposes that cells first undergo neural induction ("activation") to form default anterior neural fates and caudal regions of motor neurons are generated by induction under caudalising signals such as RA and ventralizing factor SHH ("transformation") (Mangold 1933; Stern 2001; Nieuwkoop and Nigtevecht 1954). In vitro step-wise differentiation of motor neuron progenitors (MNPs) commonly contains two major steps. hPSCs are first differentiated into neuroepithelial (NE) cells within 2 weeks, then NE cells are specified to MNPs in the presence of RA and SHH (Li et al. 2005; Lee et al. 2007; Du et al. 2015; Hu and Zhang 2009). Meanwhile, dual-SMAD inhibitors are used to increase the differentiation efficiency of NE cells and shorten the differentiation time (Chambers et al. 2009). However, the most caudal markers characterized in those studies are relative to hindbrain and cervical region of anterior spinal cord (Sances et al. 2016). Mechanistic studies also reveal that RA treatment leads to the binding of retinoic acid receptors (RARs) to *Hox1-5* chromatin domains (Mazzoni et al. 2013; Mahony et al. 2011). Increasing evidences have indicated that posterior spinal cord has a distinct developmental origin from NMPs (Tzouanacou et al. 2009; Gouti et al. 2014; Wind et al. 2021; Metzis et al. 2018; Gouti et al. 2017; Attardi et al. 2019; Gonzalez-Gobartt et al. 2021; Libby et al. 2021). Human spinal cord neural stem cells have been generated from hPSCs through a transient stage of hNMP, but the efficiency of SOX2 and Brachyury (T) double positive hNMPs is only around 50% (Kumamaru et al. 2018), raising the potential safety concerns. In this study, we have optimized hNMPs differentiation system and obtained over 90% efficiency (Fig. 1). Importantly, this protocol is stable and reproducible due to optimized seeding density and standard operation procedures which could facilitate its clinical usage. The hSCNPCs can be derived from hNMPs and exhibit spinal cord specific features by expressing NKX6-1, NKX2-2 and OLIG2 with continuously passage property in vitro (Fig. 1).

As one of the vital cell types in the spinal cord, motor neurons (MNs) are of great clinical importance in spinal cord injury as well as motor neuron diseases such as ALS and SMA (Sances et al. 2016; Fujimori et al. 2018; Olmsted et al. 2021; Wang et al. 2013). Conventionally, differentiation of postmitotic motor neuron has disadvantages in time consumption, low efficiency and particularly incapable of making caudal spinal motor neurons (Hu and Zhang 2009; Sances et al. 2016). The hSCNPCs based spinal motor neuron differentiation is robust and only takes 18 days to generate ChAT and VAChT positive mature spinal motor neurons, and these cells express posterior spinal cord HOX markers such as HOXC9 and HOXD11 (Fig. 2). Furthermore, the whole-cell patch-clamp and HD-MEA recordings showed that the hSCNPCs-derived spinal motor neurons can fire single AP as early as 6 days of differentiation and over 80% cells can fire APs at day 18. By day 30, the membrane properties of spinal motor neurons reach to the most mature function (Fig. 3). HD-MEA analyses also showed a consistent maturation pattern as patch-clamp electrophysiology illustrated (Fig. 3).

Several studies have reported that hPSCs-derived NMP cells can be used to generate spinal cord neural progenitor cells and these progenitors can be differentiated into spinal motor neurons with posterior regional identities (Cooper et al. 2022; Kumamaru et al. 2018; Wind and Tsakiridis 2021; Olmsted et al. 2022). To compare the regional identities of these methods-derived cells with our cells, we made a table and showed how the *HOX* genes expression were characterized (Table S1). The majority of these studies characterized the *HOX* genes expression through RT-qPCR, whereas we have performed RT-qPCR and immunostaining and measured the percentages of cells expressing different HOX proteins from HOX4 to HOX11. Therefore, this study provides a comprehensive identification of spinal motor neurons differentiated from NMPs-derived neural progenitor cells at the protein level.

In motor neuron diseases, the core synapse and therapeutic relevant structure is the neuromuscular junction (NMJ) (Picchiarelli et al. 2019; Kariya et al. 2014). In vitro modeling of NMJ has been challenging, which demands proper juxtaposition of both spinal motor neuron and skeletal muscle differentiation (Guo et al. 2011; Martins et al. 2020; Bakooshli et al. 2019; Osaki et al. 2020). The established protocols for generating NMJ in vitro can hardly form pretzel-shaped NMJ structures. By optimizing the C2C12 differentiation process, we showed that the AChR cluster formation begins at day 4 and degenerates at day 8 of in vitro differentiation (Fig. 4). Moreover, we also have established a protocol to differentiate hSCNPCs into 3D spinal motor neuron spheroids which can better mimic the positional relation between spinal motor neurons and skeletal muscle fibers (Fig. 5). Spinal motor neurons and skeletal muscle fibers favor different culture conditions (Barbeau et al. 2020). For example,

Xu *et al. Cell Regeneration*   (2023) 12:15

Page 15 of 21

muscle fiber differentiation needs horse serum whereas serum does not benefit neural differentiation. Thus, we have systematically screened different co-culture conditions, and have found that DMED medium supplemented with Ultroser™ G serum substitute is most suitable for co-culture of hSCNPCs-derived spinal motor neuron spheroids and C2C12-derived muscle fibers. Finally, we have obtained an efficient co-culture system for spinal motor neurons and skeletal muscles, and reproduced NMJ-like structures in vitro (Fig. 6).

Adult mammals have limited regeneration of CNS, while stem cells-derived NPCs hold promises to restoring functional neural circuits in vivo (Varadarajan et al. 2022). Studies of cell transplantation therapy of SCI also provide evidences of motor neuron progenitors on the recovery of locomotor functions (Kumamaru et al. 2018; Kadoya et al. 2016; Kumamaru et al. 2019; Ceto et al. 2020). The hSCNPCs-derived from high-purity hNMPs and exhibit spinal cord specific properties, and can be largely expanded to meet the need of high-volume cell transplantation. Besides, the ability to form NMJ and 3D sophistical structure would facilitate the mechanistic studies of human spinal motor neurons in development and disease. We expect the availability of hSCNPCs will hold great potential for regenerative medicine and translational study.

Methods

hPSCs culture

Human embryonic stem cells (H9) (Thomson et al. 1998) was obtained from WiCell Research Institute. Human induced pluripotent stem cells (DC60-3, DC87-3) were generated from human peripheral blood mononuclear cells (PBMNC) in our lab previously (Tao et al. 2020). Undifferentiated hPSCs were cultured in mTeSR1™ medium (STEMCELL Technologies) on Matrigel (Corning, hESCs-qualified)-coated cell culture plates. mTeSR1™ medium was changed every day and hPSCs clones were disassociated into small clumps with ReLeSR (STEMCELL Technologies) as required and passaged every 3-4 days.

Generation of human neuromesodermal progenitors from hPSCs

hPSCs (H9, DC60-3 and DC87-3) were disassociated into single cells with Accutase (Gibco) for 6-10 min at 37 ℃ incubator. hPSCs single cell suspension were counted and plated at a density of 45,000 cells/cm^2 in mTeSR1™ medium on Matrigel (Corning)-coated cell culture plates for 1 day, then cell culture medium was changed into hNMP differentiation medium at the second day and culture medium was changed every day up to day 4. One hundred ml of hNMP differentiation medium composited with 47.5 ml of DMEM/F12 (Gibco), 47.5 ml of Neurobasal (Gibco), 1 ml of N2 (STEMCELL Technologies, 100X), 2 ml of NeuroCult™ SM1 Without Vitamin A (STEMCELL Technology, 50X), 1 ml of NEAA (Gibco), 1 ml of GlutaMAX (Gibco), 20 ng/ml FGF-2 (PeproTech), 3 μM CHIR99021 (Selleck), 10 μM SB431542 (Selleck), 20 μM Dorsomorphin (Selleck).

Generation of human spinal cord neural progenitor cells from hNMPs

hNMPs were disassociated into single cells with Accutase (Gibco), and plated at a density of 100,000 cells/cm^2 in hSCNPCs induction medium on Matrigel-coated cell culture plates. hSCNPCs induction medium was changed every day up to day 6. One hundred ml of hSCNPCs induction medium composited with 47.5 ml of DMEM/F12 (Gibco), 47.5 ml of Neurobasal (Gibco), 1 ml of N2 (STEMCELL Technologies, 100X), 2 ml of NeuroCult™ SM1 Without Vitamin A (STEMCELL Technology, 50X), 1 ml of NEAA (Gibco), 1 ml of GlutaMAX (Gibco), 100 ng/ml FGF-2 (PeproTech), 100 ng/ml FGF-8 (PeproTech), 4 μM CHIR99021 (Selleck), 10 μM SB431542 (Selleck), 20 μM Dorsomorphin (Selleck), 0.2 μM Compound E (Sigma-Aldrich).

hSCNPCs culture

hSCNPCs were cultured in N2B27 medium supplemented with 2 μM SB431542, 3 μM CHIR99021, 0.25 μM Purmorphamine, 1X NEAA (Gibco), 1X GlutaMAX (Gibco) and 0.1 mM 2-Mercaptoethanol (Sigma-Aldrich), on Matrigel (Corning)-coated cell culture plates. hSCNPCs were dissociated into single cells with Accutase (Gibco), and were plated on Matrigel (Corning)-coated plates in a density of 300,000/cm^2 in hSCNPCs maintenance medium.

Spinal motor neuron differentiation from hSCNPCs

To differentiate hSCNPCs into motor neurons, hSCNPCs were dissociated into single cells with Accutase, counted and plated at a density of 100,000/cm^2 on pre-treated dish (Dish pre-treated with PDL coated for 2 hours, washed 3 times with sterilized water and then Matrigel coated for 2 hours). One hundred ml of motor neuron differentiation medium composited with 47.5 ml of DMEM/F12 (Gibco), 47.5 ml of Neurobasal (Gibco), 1 ml of N2 (STEMCELL Technologies, 100X), 2 ml of NeuroCult™ SM1 Without Vitamin A (STEMCELL Technology, 50X), 1 ml of NEAA (Gibco), 1 ml of GlutaMAX (Gibco), 1 μM Purmorphamine, 0.2 μM Compound E, 10 ng/ml BDNF, 10 ng/ml GDNF, 10 ng/ml NT-3. Ten μM Y27632 was added at the plating day. The motor neuron differentiation medium was changed every other day.

Xu *et al. Cell Regeneration*   (2023) 12:15

Page 16 of 21

Spontaneous differentiation of hSCNPCs

hSCNPCs were dissociated into single cells with Accutase (Gibco), and were plated at a density of 100,000/cm^2 on pre-treated dish (Dishes were pre-treated with PDL for 2 hours, washed 3 times with sterilized water and then re-coated with Matrigel for 2 hours). One hundred ml of spontaneous differentiation medium composited with 47.5 ml of DMEM/F12 (Gibco), 47.5 ml of Neurobasal (Gibco), 1 ml of N2 (STEMCELL Technologies, 100X), 2 ml of NeuroCult™ SM1 Without Vitamin A (STEMCELL Technology, 50X), 1 ml of NEAA (Gibco), 1 ml of GlutaMAX (Gibco). Ten µM Y27632 was added at the plating day. The spontaneous differentiation medium was changed every other day.

3D spinal motor neuron spheroids differentiation from hSCNPCs

To generate 3D spinal motor neuron spheroids, hSCNPCs were digested into single cells with Accutase (Gibco), counted and distributed into V-bottom 96-well plate at a density of 50,000/well. 3D spinal motor neuron spheroids were differentiated in N2B27 medium contains Purmorphamine, Compound E, BDNF, GDNF, NT-3 and CultureOne™ supplement (Gibco). Differentiation medium was changed every other day.

C2C12 maintenance and differentiation

C2C12 myoblasts were cultured in high-glucose DMEM medium with 10% FBS. The medium was changed every other day. To differentiate C2C12 into muscle fibers, C2C12 were dissociated into single cells with 0.05% trypsin, counted and plated in 45,000 cells/cm^2 on pre-coated dishes (Dishes were pre-treated with PDL for 2 hours, washed 3 times with sterilized water and then re-coated with Laminin for 2 hours) in C2C12 maintenance medium. On the following day, the C2C12 maintenance medium was replaced with differentiation medium (DMEM with 2% horse serum). Then the differentiation medium was changed every other day.

Co-culture of spinal motor neuron spheroids and C2C12-derived muscle fibers

To co-culture spinal motor neurons spheroids with C2C12-derived muscle fibers, we pre-differentiated C2C12 as described above. After 4 days of C2C12 differentiation, the C2C12 differentiation medium was aspirated and spinal motor neuron spheroids pre-differentiated for 12 days were plated onto C2C12-derived muscle fibers, then cultured in the incubator for 10 min without adding medium. After 10 min, the spinal motor neuron spheroids were attached on the muscle fibers, slowly adding co-culture medium (DMEM supplemented with 0.4% Ultroser™ G and 10 ng/ml BDNF and 10 ng/ml GDNF and 10 µg/ml insulin. The co-culture medium was changed every other day.

Electrophysiology of spinal motor neurons

Whole-cell patch-clamp recordings were performed as previously described (Zhang et al. 2020). hPSCs-derived spinal motor neurons were cultured in a 35 mm petri dish. For recording, the neurons were perfused with the ACSF solution (in mM): 126 NaCl, 4.9 KCl, 1.2 KH$_2$PO$_4$, 2.4 MgSO$_4$, 2.5 CaCl$_2$, 26 NaHCO$_3$, 20 Glucose. Recording pipettes (8-10 MΩ) were fabricated using a P1000 micropipette puller (Sutter Instrument, USA) and filled with internal solution consisting of (in mM): 136 K-gluconate, 6 KCl, 1 EGTA, 2.5 Na$_2$ATP, 10 HEPES. For recording action potentials, cells were recorded at a holding potential of -70 mV and a series of step depolarizing currents were injected into cells in a current-clamp mode. All the recordings were performed using an Olympus microscope (BX51WI). The data were sampled at 10 Hz and collected with a low-pass filter at 2 kHz and analyzed using the Axopatch1500B amplifier and pCLAMP10 software (Molecular Devices) and GraphPad Prism 8.0.2.

HD-MEA recordings and analysis of hSCNPCs-derived spinal motor neurons

To analyze the function of hSCNPCs-derived motor neurons, we used high-content microelectrode array system (MaxOne System, MaxWell Biosystems AG, Switzerland). MaxOne chips were pre-coated with 1% Terg-a-zyme (Sigma) overnight at room temperature and washed 3 times with sterile ddH$_2$O, then transfered MaxOne Chips in a beaker filled with 75% ethanol for 1 hour in a biological safety cabinet, and then washed 3 times with sterile ddH$_2$O, then 500 µl PDL was added for coating MaxOne chips for 2 hours at 37 °C, then washed 3 times with sterile ddH$_2$O and re-coated MaxOne chips with Matrigel (Corning) for 2 hours at 37 °C. hSCNPCs were dissociated into single cells, counted and plated on MaxOne chips at a density of 300,000 cells/chip in motor neuron differentiation medium. MEA data recording started after 6 days of plating and measured every 6 days till day 42.

For MEA data recording, MaxLab Live Software (v.21.1.2. MaxWell Biosystems AG, Switzerland) was used. Assays were chosen from assay gallery which contains three assays, activity scan, network and axon recording. To be able to track axons, we first recorded the whole MaxOne HD-MEA surface using the "Activity Scan Assay" module, featured in the MaxLab Live software (MaxWell Biosystems AG, Zurich, Switzerland). Twenty nine electrode configurations, including a total of 26,400 electrodes at a distance of 17.5 µm, were used to record the spontaneous neuronal electrical activity

Xu *et al. Cell Regeneration*   (2023) 12:15

Page 17 of 21

across the entire MaxOne HD-MEA. Each electrode configuration was recorded for 60 seconds.

In a next step, axonal signals were identified with the "Axon Tracking Assay" module of the MaxLab Live software, which uses a tailored recording strategy similar to the ones described in previous publications (Bakkum et al. 2013; Radivojevic et al. 2017; Bullmann et al. 2019). First, a set of 30 target neurons was identified by selecting the positions of 30 electrodes featuring the largest spike amplitude, keeping a minimum distance of 17.5 μm between each two target neurons. For every target neuron, a 3×3 electrodes block (distance between electrodes 17.5 μm) was selected around the central electrode. After defining the 3×3 blocks, a set of sequential 180 s recordings that covered larger array areas (300×300 to 800×800 μm^2 around the blocks) was run, where the 3×3 central blocks were always included in every recording.

The detected spikes on the 3×3 electrode blocks were then sorted using a K-Means clustering algorithm (Lewicki 1998) based on the action potential minimum spike amplitude. Spike sorting results were used to reconstruct the spike-triggered average extracellular waveform over the recorded array area for every identified neuron. An unsupervised object-tracking algorithm was then used to detect the path of action potential signal propagation, thus identifying (1) individual axonal branches and (2) the morphology of neuronal outgrowth per cell. The axonal conduction velocity was then calculated for every detected axonal branch.

Immunocytochemistry

Cells were fixed with 4% paraformaldehyde (PFA, Sigma-Aldrich) for 20 minutes at room temperature then washed 3 times with PBS. Cells were blocked with 0.3% Triton X-100 /5% fetal bovine serum in PBS for 1 hour at room temperature. Primary antibodies were diluted in 0.3% Triton X-100 /5% fetal bovine serum in PBS and incubated overnight at 4°C. Samples were washed in PBS for three times and then incubated with secondary antibodies (1:200-1:1000) in 0.3% Triton X-100 /5% fetal bovine serum in PBS for 2 hours. Images were taken with Leica TCS SP8 confocal laser-scanning microscope.

RT-qPCR analysis

Total RNA was extracted from cultured cells by using the TRIzol reagent, and cDNA was reverse-transcribed, starting from 1000 ng of total RNA with the SuperScript III First-strand cDNA synthesis kit (Invitrogen). qPCR was performed using Mastercycler RealPlex2 (Eppendorf) and Stormstar SYBR Green qPCR MasterMix (DBI Bioscience). Data were normalized for GAPDH expression. The primers sequences used for qPCR amplification were listed in Table S2.

RNA-sequencing and data analysis

Cell samples at different stages were collected and mRNA-seq libraries were constructed with NEBNext® Ultra™ II Library Prep Kit for Illumina. Qualified libraries were multiplexed and sequenced on Illumina NovaSeq 6000 according to the manufacturer's instructions (Illumina, USA). The Sequencing mode was PE150.

For data analysis, reference genome and gene annotation files were downloaded from GENECODE (hg38). Fastq files were pre-processed by Fastp (v0.12.1) (Chen et al. 2018) with default parameters. Cleaned data were then aligned to the reference genome via Hisat2 (v2.1.0) (Kim et al. 2015). FeatureCounts (v1.5.3) (Liao et al. 2014) was used to count the reads mapped to each gene.

Correlation to nmps

RNA-seq data in this paper were compared with nmps (Verrier et al. 2018) after removing batch effects by the R package "ComBat" (Johnson et al. 2007). Principal Components Analysis (PCA) (Jolliffe 2002) was used to show the correlation of these samples.

Correlation to BRAINSPAN database and pseudo-bulk RNA-seq of human single cell spinal cord

The 'Developmental Transcriptome Dataset' of BRAIN-SPAN (https://www.brainspan.org/static/download.html) was also downloaded. We merged the brain samples of same stage and calculated Pearson correlation coefficients between the merged samples and RNA-seq data in this paper.

Pseudo-bulk RNA-seq of human spinal cord, GSE171892 (Rayon et al. 2021), was conducted through the R package "scuttle" (McCarthy et al. 2017). After that, samples at same stages were merged and Pearson correlation coefficients were calculated between the pseudo-bulk RNA-seq and RNA-seq data in this paper.

Inference of regulons and their activity

The SCENIC (Aibar et al. 2017) was used to infer the gene regulatory network (regulon). Binary regulon-activity matrix for all samples was used in principal components analysis. GO enrichment analysis of related target genes was carried out by Metascape (https://metascape.org/) with default parameters (Zhou et al. 2019).

Statistical analysis

All statistical analyses were performed in GraphPad Prism software (GraphPad Prism 8.0.2). Cell counting, RT-qPCR data and electrophysiological data were presented as mean ± SD. Student's t test (two-tailed) was

Xu *et al. Cell Regeneration*   (2023) 12:15

Page 18 of 21

performed for statistical analysis between two groups. Sample size (n) values were provided in the relevant text, figures, and figure legends. The statistical analyses were obtained from three independent experiments. Statistical significance was set at *p* values.

Data availability

All RNA-seq data are available at the Gene Expression Omnibus (GEO) under accession number GSE205718.

Abbreviations

ALS	Amyotrophic lateral sclerosis
SMA	Spinal muscular atrophy
SCI	Spinal cord injury
hPSCs	Human pluripotent stem cells
hSCNPCs	Human spinal cord neural progenitor cells
NMPs	Neuromesodermal progenitors
NMJ	Neuromuscular junction
MNs	Motor neurons
AP	Anterior-posterior
NE	Neuroepithelial
EB	Embryonic body
MNPs	Motor neuron progenitors
RA	Retinoic acid
SHH	Sonic hedgehog
CNS	Central nervous system
CLE	Caudal lateral epiblasts
T	Brachyury
PCA	Principal component analysis
NeuDet	Neural determination
GO	Gene Ontology
BDNF	Brain-derived neurotrophic factor
GDNF	Glial cell line-derived neurotrophic factor
NT-3	Neurotrophin-3
SST	Somatostatin
HD-MEA	High-density microelectrode array
APs	Action potentials
RMPs	Resting membrane potentials
Rin	Resistance
MRF	Mean firing rate
sPSC	Spontaneous postsynaptic currents
SYP	Synaptophysin
MyHC	Myosin heavy chain
α-BTX	α-bungarotoxin
HS	Horse serum
UG	Ultroser G
RARs	Retinoic acid receptors

Supplementary Information

The online version contains supplementary material available at https://doi.org/10.1186/s13619-023-00159-6.

Additional file 1: Fig. S1. Characterization of hNMPs and hSCNPCs from hPSCs. (A) Immunofluorescent staining of hNMP marker (CDX2) and the quantification results. Scale bar, 50 μm. *n* = 3 independent experiments. Data are represented as mean ± SD. (B) Immunofluorescent staining of hNMP markers (SOX2 and Brachyury) of hiPSCs (DC60-3 and DC87-3)-derived NMPs and the quantification results. Scale bar, 50 μm. n = 3 independent experiments. Data are represented as mean ± SD. (C) Immunofluorescent staining of hNMP marker (CDX2) of hiPSCs (DC60-3 and DC87-3)-derived NMPs and the quantification results. Scale bar, 50 μm. n = 3 independent experiments. Data are represented as mean ± SD. (D) Relative marker genes expression of during NeuDet stage. n = 3 independent experiments. Data are represented as mean ± SD. (E) Karyotyping of hSCNPCs at P40. (F) Immunofluorescence analysis of

---

hiPSCs (DC60-3 and DC87-3)-derived hiSCNPCs and the quantification results. Scale bar, 50 μm. n = 3 independent experiments. Data are represented as mean ± SD. **Fig. S2.** RNA expression pattern during spinal motor neuron differentiation and characterization of hiSCNPCs-derived spinal motor neurons. (A) Relative marker genes expression during spinal motor neuron differentiation from hSCNPCs. n = 3 independent experiments. Data are represented as mean ± SD. (B) Immunostaining characterization of hiSCNPCs (Derived from hiPSCs lines DC60-3 and DC87-3) differentiated spinal motor neurons at day 18. Scale bar, 50 μm. (C) The heat-map showing two regulon groups in samples of spinal motor neuron differentiation from hSCNPCs with listing representative regulon transcription factors (numbers of predicted target genes by SCENIC in the brackets) and enriched GO terms for each regulon group. **Fig. S3.** Multipotency of hSCNPCs and efficiency of hSCNPCs differentiate into posterior spinal motor neurons. (A) Bright field of hSCNPCs spontaneous differentiated neurons. Scale bar, 500 μm. (B) Immunofluorescent staining of hSCNPCs spontaneous differentiated neurons with neuronal marker TUJ1. Scale bar, 100 μm. (C) Comparison of mir-218-2 expression levels during hSCNPCs spinal motor neuron differentiation and spontaneous differentiation. n = 3 independent experiments. Data are represented as mean ± SD. (D) Immunostaining characterization of hSCNPCs with motor neuron marker (HB9), interneuron marker (GABA, SST) and astrocyte marker (S100β). Scale bar, 50 μm. (E) Double staining of mature motor neuron marker (SMI-32) and posterior marker (HOXC9) at DIV 18. Scale bar, 50 μm. (F) Quantification of markers expression in panel E. **Fig. S4.** Characterization and quantification of hSCNPCs-differentiated motor neurons at P40. (A) Immunofluorescent staining of motor neuron markers of hSCNPCs (P40)-differentiated motor neurons. Scale bar, 100 μm. (B) Quantification of markers expression in panel A. (C) Double staining of mature motor neuron marker (SMI-32) and posterior marker (HOXC9). Scale bar, 50 μm. (D) Quantification of markers expression in panel C. **Fig. S5.** Electrophysiology of hSCNPCs differentiated spinal motor neurons. (A) Bright field illustration of motor neuron under patch clamping. Scale bar, 50 μm. (B) Immunofluorescent staining of TUJ1 and SMI-32 of spinal motor neurons co-culture with astrocyte at day 30. Scale bar, 50 μm. (C) Sample AP traces in response to a series of step current injections from 0 pA to 60 pA. (D) sPSCs of hSCNPCs are not observed in differentiated spinal motor neurons at day 30. **Fig. S6.** Generation of C2C12 myogenic differentiation. (A) Schematic illustration of C2C12 SOP myogenic differentiation scheme. (B) Immunofluorescent staining of mature muscle marker (MyHC) and acetylcholine receptor accumulation (α-BTX). Scale bar, 200 μm. (C) Representative AChR images at C2C12 differentiated cell at day 6. Scale bar, 50 μm.

Additional file 2: Table S1. Methods for the identification of HOX genes expression in human NMP-derived neuronal cells.

Additional file 3: Table S2. Oligonucleotide sequences, related to STAR Methods.

Authors' contributions
H.X. and N.J. conceived the project. H.X., Y.Y. and M.L performed the experiments and collected the data. H.X. and Y.Y. designed the experiments, analyzed the data and made figs. F.Y. and S.H. performed patch-clamp electrophysiology. X.Y. produced and J.C. and F.L. analyzed the RNA-seq data. S.L. and P.H. cultured C2C12 cells and provide assistance for C2C12 muscular differentiation. H.X., G.P. and N.J. wrote the manuscript. N.J. supervised the study. All authors read and approved the final manuscript.

Xu *et al. Cell Regeneration*   (2023) 12:15

Page 19 of 21

Availability of data and materials

All data supporting the findings of this study are available within the article and its supplementary information files or from the corresponding upon reasonable request.

Declarations

Ethics approval and consent to participate

Not applicable.

Consent for publication

Not applicable.

Competing interests

Naihe Jing is a member of the Editorial Board for Cell Regeneration. He was not involved in the journal's review of, or decisions related to this manuscript.

References

Aibar S, González-Blas CB, Moerman T, Huynh-Thu VA, Imrichova H, Hulselmans G, et al. SCENIC: single-cell regulatory network inference and clustering. Nat Methods. 2017;14(11):1083–6. https://doi.org/10.1038/nmeth.4463.

Amin ND, Bai G, Klug JR, Bonanomi D, Pankratz MT, Gifford WD, et al. Loss of motoneuron-specific microRNA-218 causes systemic neuromuscular failure. 2015;350(6267):1525–9. https://doi.org/10.1126/science.aad2509.

Amin ND, Senturk G, Costaguta G, Driscoll S, O'Leary B, Bonanomi D, et al. A hidden threshold in motor neuron gene networks revealed by modulation of miR-218 dose. Neuron. 2021;109(20):3252–67 e6. https://doi.org/10.1016/j.neuron.2021.07.028.

Attardi A, Fulton T, Florescu M, Shah G, Muresan L, Lenz MO, et al. Correction: Neuromesodermal progenitors are a conserved source of spinal cord with divergent growth dynamics (doi: 10.1242/dev.166728). Development. 2019;146(2). https://doi.org/10.1242/dev.175620.

Bakkum DJ, Frey U, Radivojevic M, Russell TL, Muller J, Fiscella M, et al. Tracking axonal action potential propagation on a high-density microelectrode array across hundreds of sites. Nat Commun. 2013;4:2181. https://doi.org/10.1038/ncomms3181.

Bakooshli MA, Lippmann ES, Mulcahy B, Iyer N, Nguyen CT, Tung K, et al. A 3D culture model of innervated human skeletal muscle enables studies of the adult neuromuscular junction. 2019;8:e44530. https://doi.org/10.7554/elife.44530.033.

Barbeau S, Tahraoui-Bories J, Legay C, Martinat C. Building neuromuscular junctions in vitro. Development. 2020;147(22):dev193920. https://doi.org/10.1242/dev.193920.

Ben-Shushan E, Feldman E, Reubinoff BE. Notch signaling regulates motor neuron differentiation of human embryonic stem cells. Stem Cells. 2015;33(2):403–15. https://doi.org/10.1002/stem.1873.

Bullmann T, Radivojevic M, Huber ST, Deligkaris K, Hierlemann A, Frey U. Large-scale mapping of axonal arbors using high-density microelectrode arrays. Front Cell Neurosci. 2019;13:404. https://doi.org/10.3389/fncel.2019.00404.

Ceto S, Sekiguchi KJ, Takashima Y, Nimmerjahn A, Tuszynski MH. Neural stem cell grafts form extensive synaptic networks that integrate with host circuits after spinal cord injury. Cell Stem Cell. 2020;27(3):430–40. e5. https://doi.org/10.1016/j.stem.2020.07.007.

Chambers SM, Fasano CA, Papapetrou EP, Tomishima M, Sadelain M, Studer L. Highly efficient neural conversion of human ES and iPS cells by dual inhibition of SMAD signaling. Nat Biotechnol. 2009;27(3):275–80. https://doi.org/10.1038/nbt.1529.

Chapman DL, Papaioannou VE. Three neural tubes in mouse embryos with mutations in the T-box gene Tbx6. Nature. 1998;391(6668):695–7. https://doi.org/10.1038/35624.

Chen S, Zhou Y, Chen Y, Gu J. Fastp: an ultra-fast all-in-one FASTQ preprocessor. Bioinformatics (Oxford, England). 2018;34(17):i884–i90. https://doi.org/10.1093/bioinformatics/bty560.

Clowry G, Sieradzan K, Vrbová G. Transplants of embryonic motoneurones to adult spinal cord: survival and innervation abilities. Trends Neurosci. 1991;14(8):355–7. https://doi.org/10.1016/0166-2236(91)90162-n.

Cooper F, Gentsch GE, Mitter R, Bouissou C, Healy LE, Rodriguez AH, et al. Rostrocaudal patterning and neural crest differentiation of human pre-neural spinal cord progenitors in vitro. Stem Cell Rep. 2022;17(4):894–910. https://doi.org/10.1016/j.stemcr.2022.02.018.

Cutarelli A, Martinez-Rojas VA, Tata A, Battistella I, Rossi D, Arosio D, et al. A monolayer system for the efficient generation of motor neuron progenitors and functional motor neurons from human pluripotent stem cells. Cells. 2021;10(5). https://doi.org/10.3390/cells10051127.

Dasen JS, Tice BC, Brenner-Morton S, Jessell TM. A Hox regulatory network establishes motor neuron pool identity and target-muscle connectivity. Cell. 2005;123(3):477–91. https://doi.org/10.1016/j.cell.2005.09.009.

Davis-Dusenbery BN, Williams LA, Klim JR, Eggan K. How to make spinal motor neurons. Development. 2014;141(3):491–501. https://doi.org/10.1242/dev.097410.

De Marco Garcia NV, Jessell TM. Early motor neuron pool identity and muscle nerve trajectory defined by postmitotic restrictions in Nkx6.1 activity. Neuron. 2008;57(2):217–31. https://doi.org/10.1016/j.neuron.2007.11.033.

Du ZW, Chen H, Liu H, Lu J, Qian K, Huang CL, et al. Generation and expansion of highly pure motor neuron progenitors from human pluripotent stem cells. Nat Commun. 2015;6:6626. https://doi.org/10.1038/ncomms7626.

Ebert AD, Svendsen CN. Human stem cells and drug screening: opportunities and challenges. Nat Rev Drug Discov. 2010;9(5):367–72. https://doi.org/10.1038/nrd3000.

Fujimori K, Ishikawa M, Otomo A, Atsuta N, Nakamura R, Akiyama T, et al. Modeling sporadic ALS in iPSC-derived motor neurons identifies a potential therapeutic agent. Nat Med. 2018;24(10):1579–89. https://doi.org/10.1038/s41591-018-0140-5.

Gonzalez-Gobartt E, Blanco-Ameijeiras J, Usieto S, Allio G, Benazeraf B, Marti E. Cell intercalation driven by SMAD3 underlies secondary neural tube formation. Dev Cell. 2021;56(8):1147–63 e6. https://doi.org/10.1016/j.devcel.2021.03.023.

Gouti M, Tsakiridis A, Wymeersch FJ, Huang Y, Kleinjung J, Wilson V, et al. In vitro generation of neuromesodermal progenitors reveals distinct roles for wnt signalling in the specification of spinal cord and paraxial mesoderm identity. PLoS Biol. 2014;12(8):e1001937. https://doi.org/10.1371/journal.pbio.1001937.

Gouti M, Delile J, Stamataki D, Wymeersch FJ, Huang Y, Kleinjung J, et al. A gene regulatory network balances neural and mesoderm specification during vertebrate trunk development. Dev Cell. 2017;41(3):243–61 e7. https://doi.org/10.1016/j.devcel.2017.04.002.

Guo X, Gonzalez M, Stancescu M, Vandenburgh HH, Hickman JJ. Neuromuscular junction formation between human stem cell-derived motoneurons and human skeletal muscle in a defined system. Biomaterials. 2011;32(36):9602–11. https://doi.org/10.1016/j.biomaterials.2011.09.014.

Guthrie S. Neuronal development: putting motor neurons in their place. Curr Biol. 2004;14(4):R166–R8. https://doi.org/10.1016/j.cub.2004.01.050.

Henrique D, Abranches E, Verrier L, Storey KG. Neuromesodermal progenitors and the making of the spinal cord. Development. 2015;142(17):2864–75. https://doi.org/10.1242/dev.119768.

Hester ME, Murtha MJ, Song S, Rao M, Miranda CJ, Meyer K, et al. Rapid and efficient generation of functional motor neurons from human pluripotent stem cells using gene delivered transcription factor codes. Mol Ther. 2011;19(10):1905–12. https://doi.org/10.1038/mt.2011.135.

Hoye ML, Regan MR, Jensen LA, Lake AM, Reddy LV, Vidensky S, et al. Motor neuron-derived microRNAs cause astrocyte dysfunction in amyotrophic lateral sclerosis. Brain. 2018;141(9):2561–75. https://doi.org/10.1093/brain/awy182.

Hu BY, Zhang SC. Differentiation of spinal motor neurons from pluripotent human stem cells. Nat Protoc. 2009;4(9):1295–304. https://doi.org/10.1038/nprot.2009.127.

Hudish LI, Bubak A, Triolo TM, Niemeyer CS, Lorberbaum DS, Sussel L, et al. Modeling hypoxia-induced neuropathies using a fast and scalable human motor neuron differentiation system. Stem Cell Rep. 2020;14(6):1033–43. https://doi.org/10.1016/j.stemcr.2020.04.003.

Xu *et al. Cell Regeneration*   (2023) 12:15

Page 20 of 21

Johnson WE, Li C, Rabinovic A. Adjusting batch effects in microarray expression data using empirical Bayes methods. Biostatistics (Oxford, England). 2007;8(1):118–27. https://doi.org/10.1093/biostatistics/kxj037.

Jolliffe IT. Principal component analysis for special types of data: Springer; 2002. https://doi.org/10.1007/0-387-22440-8_13.

Kadoya K, Lu P, Nguyen K, Lee-Kubli C, Kumamaru H, Yao L, et al. Spinal cord reconstitution with homologous neural grafts enables robust corticospinal regeneration. Nat Med. 2016;22(5):479–87. https://doi.org/10.1038/nm.4066.

Kanning KC, Kaplan A, Henderson CE. Motor neuron diversity in development and disease. Annu Rev Neurosci. 2010;33:409–40. https://doi.org/10.1146/annurev.neuro.051508.135722.

Karagiannis P, Takahashi K, Saito M, Yoshida Y, Okita K, Watanabe A, et al. Induced pluripotent stem cells and their use in human models of disease and development. 2019;99(1):79–114. https://doi.org/10.1152/physrev.00039.2017.

Kariya S, Obis T, Garone C, Akay T, Sera F, Iwata S, et al. Requirement of enhanced survival Motoneuron protein imposed during neuromuscular junction maturation. J Clin Invest. 2014;124(2):785–800. https://doi.org/10.1172/jci72017.

Kim D, Langmead B, Salzberg SL. HISAT: a fast spliced aligner with low memory requirements. Nat Methods. 2015;12(4):357–60. https://doi.org/10.1038/nmeth.3317.

Kumamaru H, Kadoya K, Adler AF, Takashima Y, Graham L, Coppola G, et al. Generation and post-injury integration of human spinal cord neural stem cells. Nat Methods. 2018;15(9):723–31. https://doi.org/10.1038/s41592-018-0074-3.

Kumamaru H, Lu P, Rosenzweig ES, Kadoya K, Tuszynski MH. Regenerating corticospinal axons innervate phenotypically appropriate neurons within neural stem cell grafts. Cell Rep. 2019;26(9):2329–39. e4. https://doi.org/10.1016/j.celrep.2019.01.099.

Lee H, Shamy GA, Elkabetz Y, Schofield CM, Harrsion NL, Panagiotakos G, et al. Directed differentiation and transplantation of human embryonic stem cell-derived motoneurons. Stem Cells. 2007;25(8):1931–9. https://doi.org/10.1634/stemcells.2007-0097.

Lewicki MS. A review of methods for spike sorting: the detection and classification of neural action potentials. Network. 1998;9(4):R53. https://doi.org/10.1088/0954-898x_9_4_001.

Li XJ, Du ZW, Zarnowska ED, Pankratz M, Hansen LO, Pearce RA, et al. Specification of motoneurons from human embryonic stem cells. Nat Biotechnol. 2005;23(2):215–21. https://doi.org/10.1038/nbt1063.

Li XJ, Hu BY, Jones SA, Zhang YS, Lavaute T, Du ZW, et al. Directed differentiation of ventral spinal progenitors and motor neurons from human embryonic stem cells by small molecules. Stem Cells. 2008;26(4):886–93. https://doi.org/10.1634/stemcells.2007-0620.

Liao Y, Smyth GK, Shi W. featureCounts: an efficient general purpose program for assigning sequence reads to genomic features. Bioinformatics (Oxford, England). 2014;30(7):923–30. https://doi.org/10.1093/bioinformatics/btt656.

Libby ARG, Joy DA, Elder NH, Bulger EA, Krakora MZ, Gaylord EA, et al. Axial elongation of caudalized human organoids mimics aspects of neural tube development. Development. 2021;148(12). https://doi.org/10.1101/2020.03.05.979732.

Lu CC, Brennan J, Robertson EJ. From fertilization to gastrulation: axis formation in the mouse embryo. Curr Opin Genet Dev. 2001;11(4):384–92. https://doi.org/10.1016/s0959-437x(00)00208-2.

Mahony S, Mazzoni EO, McCuine S, Young RA, Wichterle H, Gifford DK. Ligand-dependent dynamics of retinoic acid receptor binding during early neurogenesis. Genome Biol. 2011;12(1):1–15. https://doi.org/10.1186/gb-2011-12-1-r2.

Mangold O. Über die Induktionsfähigkeit der verschiedenen Bezirke der Neurula von Urodelen. Naturwissenschaften. 1933;21(43):761–6. https://doi.org/10.1007/bf01503740.

Martins J-MF, Fischer C, Urzi A, Vidal R, Kunz S, Ruffault P-L, et al. Self-organizing 3D human trunk neuromuscular organoids. 2020;26(2):172–86. e6. https://doi.org/10.1016/j.stem.2019.12.007.

Mazzoni EO, Mahony S, Peljto M, Patel T, Thornton SR, McCuine S, et al. Saltatory remodeling of Hox chromatin in response to rostrocaudal patterning signals. Nat Neurosci. 2013;16(9):1191–8. https://doi.org/10.1038/nn.3490.

McCarthy DJ, Campbell KR, Lun AT, Wills QF. Scater: pre-processing, quality control, normalization and visualization of single-cell RNA-seq data in R.

Bioinformatics (Oxford, England). 2017;33(8):1179–86. https://doi.org/10.1093/bioinformatics/btw777.

Metzis V, Steinhauser S, Pakanavicius E, Gouti M, Stamataki D, Ivanovitch K, et al. Nervous system regionalization entails axial allocation before neural differentiation. Cell. 2018;175(4):1105–18 e17. https://doi.org/10.1016/j.cell.2018.09.040.

Muller J, Ballini M, Livi P, Chen Y, Radivojevic M, Shadmani A, et al. High-resolution CMOS MEA platform to study neurons at subcellular, cellular, and network levels. Lab Chip. 2015;15(13):2767–80. https://doi.org/10.1039/c5lc00133a.

Narasimhan KJ. Quantifying motor neuron loss in ALS. Nat Neurosci. 2006;9(3):304. https://doi.org/10.1038/nn0306-304.

Nieuwkoop PD, Nigtevecht GV. Neural activation and transformation in explants of competent ectoderm under the influence of fragments of anterior notochord in urodeles. 1954. https://doi.org/10.1242/dev.2.3.175.

Nijssen J, Comley LH, Hedlund E. Motor neuron vulnerability and resistance in amyotrophic lateral sclerosis. Acta Neuropathol. 2017;133(6):863–85. https://doi.org/10.1007/s00401-017-1708-8.

Olmsted ZT, Stigliano C, Marzullo B, Cibelli J, Horner PJ, Paluh JL. Fully characterized mature human iPS- and NMP-derived motor neurons thrive without Neuroprotection in the spinal contusion cavity. Front Cell Neurosci. 2022:15. https://doi.org/10.3389/fncel.2021.725195.

Olmsted ZT, Stigliano C, Scimemi A, Wolfe T, Cibelli J, Horner PJ, et al. Transplantable human motor networks as a neuron-directed strategy for spinal cord injury. iScience. 2021;24(8):102827. https://doi.org/10.1016/j.isci.2021.102827.

Osaki T, Uzel SG, Kamm RD. On-chip 3D neuromuscular model for drug screening and precision medicine in neuromuscular disease. Nat Protoc. 2020;15(2):421–49. https://doi.org/10.1038/s41596-019-0248-1.

Patani R, Hollins AJ, Wishart TM, Puddifoot CA, Alvarez S, de Lera AR, et al. Retinoid-independent motor neurogenesis from human embryonic stem cells reveals a medial columnar ground state. Nat Commun. 2011;2:214. https://doi.org/10.1038/ncomms1216.

Picchiarelli G, Demestre M, Zuko A, Been M, Higelin J, Dieterle S, et al. FUS-mediated regulation of acetylcholine receptor transcription at neuromuscular junctions is compromised in amyotrophic lateral sclerosis. Nat Neurosci. 2019;22(11):1793–805. https://doi.org/10.1038/s41593-019-0498-9.

Qu Q, Li D, Louis KR, Li X, Yang H, Sun Q, et al. High-efficiency motor neuron differentiation from human pluripotent stem cells and the function of Islet-1. Nat Commun. 2014;5:3449. https://doi.org/10.1038/ncomms4449.

Radivojevic M, Franke F, Altermatt M, Muller J, Hierlemann A, Bakkum DJ. Tracking individual action potentials throughout mammalian axonal arbors. Elife. 2017;6. https://doi.org/10.7554/elife.30198.

Rayon T, Maizels RJ, Barrington C, Briscoe J. Single-cell transcriptome profiling of the human developing spinal cord reveals a conserved genetic programme with human-specific features. Development. 2021;148(15). https://doi.org/10.1242/dev.199711.

Reichenstein I, Eitan C, Diaz-Garcia S, Haim G, Magen I, Siany A, et al. Human genetics and neuropathology suggest a link between miR-218 and amyotrophic lateral sclerosis pathophysiology. 2019;11(523):eaav5264. https://doi.org/10.1126/scitranslmed.aav5264.

Sances S, Bruijn LI, Chandran S, Eggan K, Ho R, Klim JR, et al. Modeling ALS with motor neurons derived from human induced pluripotent stem cells. Nat Neurosci. 2016;19(4):542–53. https://doi.org/10.1038/nn.4273.

Sockanathan S, Jessell TM. Motor neuron–derived retinoid signaling specifies the subtype identity of spinal motor neurons. Cell. 1998;94(4):503–14. https://doi.org/10.1016/s0092-8674(00)81591-3.

Solnica-Krezel L. Conserved patterns of cell movements during vertebrate gastrulation. Curr Biol. 2005;15(6):R213–28. https://doi.org/10.1016/j.cub.2005.03.016.

Son EY, Ichida JK, Wainger BJ, Toma JS, Rafuse VF, Woolf nduced pluripotent stem cell lines derived CJ, et al. Conversion of mouse and human fibroblasts into functional spinal motor neurons. Cell Stem Cell. 2011;9(3):205–18. https://doi.org/10.1016/j.stem.2011.07.014.

Stern CD. Initial patterning of the central nervous system: how many organizers? Nat Rev Neurosci. 2001;2(2):92–8. https://doi.org/10.1038/35053563.

Storey KG, Crossley JM, De Robertis EM, Norris WE, Stern CD. Neural induction and regionalisation in the chick embryo. Development. 1992;114(3):729–41. https://doi.org/10.1242/dev.114.3.729.

Sundberg M, Pinson H, Smith RS, Winden KD, Venugopal P, Tai DJC, et al. 16p11.2 deletion is associated with hyperactivation of human

Xu *et al. Cell Regeneration*   (2023) 12:15

Page 21 of 21

iPSC-derived dopaminergic neuron networks and is rescued by RHOA inhibition in vitro. Nat Commun. 2021;12(1):2897. https://doi.org/10.1038/s41467-021-23113-z.

Takahashi K, Tanabe K, Ohnuki M, Narita M, Ichisaka T, Tomoda K, et al. Induction of pluripotent stem cells from adult human fibroblasts by defined factors. 2007;131(5):861–72. https://doi.org/10.1016/j.cell.2007.11.019.

Tam PP, Behringer RR. Mouse gastrulation: the formation of a mammalian body plan. Mech Dev. 1997;68(1-2):3–25. https://doi.org/10.1016/s0925-4773(97)00123-8.

Tao R, Lu R, Wang J, Zeng S, Zhang T, Guo W, et al. Probing the therapeutic potential of TRPC6 for Alzheimer's disease in live neurons from patient-specific iPSCs. J Mol Cell Biol. 2020;12(10):807–16. https://doi.org/10.1093/jmcb/mjaa027.

Thomson JA, Itskovitz-Eldor J, Shapiro SS, Waknitz MA, Swiergiel JJ, Marshall VS, et al. Embryonic stem cell lines derived from human blastocysts. 1998;282(5391):1145–7. https://doi.org/10.1126/science.282.5391.1145.

Turner DA, Hayward PC, Baillie-Johnson P, Rue P, Broome R, Faunes F, et al. Wnt/beta-catenin and FGF signalling direct the specification and maintenance of a neuromesodermal axial progenitor in ensembles of mouse embryonic stem cells. Development. 2014;141(22):4243–53. https://doi.org/10.1242/dev.112979.

Tzouanacou E, Wegener A, Wymeersch FJ, Wilson V, Nicolas JF. Redefining the progression of lineage segregations during mammalian embryogenesis by clonal analysis. Dev Cell. 2009;17(3):365–76. https://doi.org/10.1016/j.devcel.2009.08.002.

Varadarajan SG, Hunyara JL, Hamilton NR, Kolodkin AL, Huberman AD. Central nervous system regeneration. Cell. 2022;185(1):77–94. https://doi.org/10.1016/j.cell.2021.10.029.

Verrier L, Davidson L, Gierlinski M, Dady A, Storey KG. Neural differentiation, selection and transcriptomic profiling of human neuromesodermal progenitor-like cells in vitro. Development. 2018;145(16). https://doi.org/10.1242/dev.166215.

Wang ZB, Zhang X, Li XJ. Recapitulation of spinal motor neuron-specific disease phenotypes in a human cell model of spinal muscular atrophy. Cell Res. 2013;23(3):378–93. https://doi.org/10.1038/cr.2012.166.

Wind M, Gogolou A, Manipur I, Granata I, Butler L, Andrews PW, et al. Defining the signalling determinants of a posterior ventral spinal cord identity in human neuromesodermal progenitor derivatives 2021;148(6):dev194415. https://doi.org/10.1242/dev.194415.

Wind M, Tsakiridis A. In vitro generation of posterior motor neurons from human pluripotent stem cells. Curr Protocols. 2021;1(9). https://doi.org/10.1002/cpz1.244.

Wymeersch FJ, Wilson V, Tsakiridis A. Understanding axial progenitor biology in vivo and in vitro. Development. 2021;148(4). https://doi.org/10.1242/dev.180612.

Yu J, Vodyanik MA, Smuga-Otto K, Antosiewicz-Bourget J, Frane JL, Tian S, et al. Induced pluripotent stem cell lines derived from human somatic cells. 2007;318(5858):1917–20. https://doi.org/10.1126/science.1151526.

Yuan X, Schroter M, Obien MEJ, Fiscella M, Gong W, Kikuchi T, et al. Versatile live-cell activity analysis platform for characterization of neuronal dynamics at single-cell and network level. Nat Commun. 2020;11(1):4854. https://doi.org/10.1038/s41467-020-18620-4.

Zhang T, Ke W, Zhou X, Qian Y, Feng S, Wang R, et al. Human neural stem cells reinforce hippocampal synaptic network and rescue cognitive deficits in a mouse model of Alzheimer's disease. Stem Cell Reports. 2019;13(6):1022–37. https://doi.org/10.1016/j.stemcr.2019.10.012.

Zhang K, Yu F, Zhu J, Han S, Chen J, Wu X, et al. Imbalance of excitatory/inhibitory neuron differentiation in neurodevelopmental disorders with an NR2F1 point mutation. Cell Rep. 2020;31(3):107521. https://doi.org/10.1016/j.celrep.2020.03.085.

Zhou Y, Zhou B, Pache L, Chang M, Khodabakhshi AH, Tanaseichuk O, et al. Metascape provides a biologist-oriented resource for the analysis of systems-level datasets. Nat Commun. 2019;10(1):1523. https://doi.org/10.1038/s41467-019-09234-6.